UNIVERSITY OF BIRMINGHAM
University of Birmingham Research at Birmingham

Vibration energy harvester for variable speed rotor applications using passively self-tuned beams

Alevras, Panagiotis; Theodossiades, Stephanos

DOI:
10.1016/j.jsv.2018.11.007

License:
Creative Commons: Attribution-NonCommercial-NoDerivs (CC BY-NC-ND)

Document Version
Peer reviewed version

Citation for published version (Harvard):
Alevras, P & Theodossiades, S 2019, 'Vibration energy harvester for variable speed rotor applications using passively self-tuned beams', *Journal of Sound and Vibration*, vol. 444, pp. 176-196. https://doi.org/10.1016/j.jsv.2018.11.007

Link to publication on Research at Birmingham portal

Publisher Rights Statement:
This is the version of the above work as accepted for publication. Final version of record available at:
https://doi.org/10.1016/j.jsv.2018.11.007

General rights
Unless a licence is specified above, all rights (including copyright and moral rights) in this document are retained by the authors and/or the copyright holders. The express permission of the copyright holder must be obtained for any use of this material other than for purposes permitted by law.

• Users may freely distribute the URL that is used to identify this publication.
• Users may download and/or print one copy of the publication from the University of Birmingham research portal for the purpose of private study or non-commercial research.
• User may use extracts from the document in line with the concept of 'fair dealing' under the Copyright, Designs and Patents Act 1988 (?)
• Users may not further distribute the material nor use it for the purposes of commercial gain.

Where a licence is displayed above, please note the terms and conditions of the licence govern your use of this document.

When citing, please reference the published version.

Take down policy
While the University of Birmingham exercises care and attention in making items available there are rare occasions when an item has been uploaded in error or has been deemed to be commercially or otherwise sensitive.

If you believe that this is the case for this document, please contact UBIRA@lists.bham.ac.uk providing details and we will remove access to the work immediately and investigate.

Download date: 01. Mar. 2020

Accepted Manuscript

Vibration energy harvester for variable speed rotor applications using passively self-tuned beams

Panagiotis Alevras, Stephanos Theodossiades

PII: S0022-460X(18)30759-4

DOI: https://doi.org/10.1016/j.jsv.2018.11.007

Reference: YJSVI 14490

To appear in: *Journal of Sound and Vibration*

Received Date: 18 June 2018

Revised Date: 1 October 2018

Accepted Date: 5 November 2018

Please cite this article as: P. Alevras, S. Theodossiades, Vibration energy harvester for variable speed rotor applications using passively self-tuned beams, *Journal of Sound and Vibration* (2018), doi: https://doi.org/10.1016/j.jsv.2018.11.007.

This is a PDF file of an unedited manuscript that has been accepted for publication. As a service to our customers we are providing this early version of the manuscript. The manuscript will undergo copyediting, typesetting, and review of the resulting proof before it is published in its final form. Please note that during the production process errors may be discovered which could affect the content, and all legal disclaimers that apply to the journal pertain.

ACCEPTED MANUSCRIPT

Vibration energy harvester for variable speed rotor applications using passively self-tuned beams

Panagiotis Alevras[1]
Wolfson School of Mechanical, Electrical & Manufacturing Engineering
Loughborough University, Loughborough, LE11 3TU, UK
P.Alevras@lboro.ac.uk

Stephanos Theodossiades
Wolfson School of Mechanical, Electrical & Manufacturing Engineering
Loughborough University, Loughborough, LE11 3TU, UK
S.Theodossiades@lboro.ac.uk

ABSTRACT

A vibration energy harvester is proposed for rotating systems based on transverse vibrations of an assembly of thin beams and electromagnetic interaction of a carried magnet with a coil of wire. The harvester is designed in a way such that centrifugal forces are utilized to tune the system's natural frequency to the expected frequency of torsional vibrations. In fact, a novel combination of a tuning mass positioned at the beam's support and an applied preload are introduced to establish a tuning mechanism that is capable of maintaining resonance along a wide frequency range. The device's tuning can cover relatively high rotor speeds, overcoming previous limitations on the size and the physics of tuning via axial loads. Moreover, exact expressions of the beams' mode shapes are taken into account to improve the accuracy of the proposed tuning mechanism. Numerical simulations of the device's response are carried out for case studies corresponding to different frequency orders. It is shown that the system can maintain a flat power output across a wide range of operating speeds, effectively leading to purely broadband energy harvesting.

KEYWORDS: Energy harvesting; Rotational; Self-tuning; Beam; Centrifugal force.

[1] Corresponding author

NOMENCLATURE

A	Area of the beams' cross-section (m^2)
A_i, B_i, C_i, D_i	Coefficients of the general mode shape formulation for the i-th beam segment (m)
B_r	Remnant magnetic field strength (T)
D_i	Inner diameter of the coil (m)
D_o	Outer diameter of the coil (m)
E	Young's modulus for each of the beams (Pa)
E_s	Young's modulus for the two beams together (Pa)
$F(t)$	External excitation force (N)
I	Current (A)
I_s	Second moment of area of the beams' cross-section (m^4)
L	Total length of each beam (m)
L_1	Position of the vibrating magnet (m)
L_2	Distance of the vibrating magnet from the far-end support (m)
L_H	Inductance (H)
$M_{1,nm}$	Non-magnetic portion of M_1 (kg)
M_1	Mass of the vibrating magnet (kg)
M_2	Tuning mass positioned at the beams' far-end support (kg)
M_t	Total lumped mass carried by the beams (kg)
N_c	Number of turns of the coil
P_{M_i}	Centrifugal force acting on M_i (N)
$P_{L,av}$	Average electrical power delivered to the load (W)
P_L	Electrical power delivered to the load (W)
P_i	Axial force acting on the beams at x_i (N)
P_{pre}	Axial pre-load (N)
R_C	Electrical resistance of the coil (Ω)

ACCEPTED MANUSCRIPT

R_L	Load resistance (Ω)
V_c	Voltage induced to the coil (V)
b_s	Width of the beams (m)
c	Mechanical damping coefficient (Ns/m)
c_b	Generalised damping coefficient (Ns/m)
$e_0(x_i, t)$	Strain due to axial deformation
$e_b(x_i, t)$	Strain due to bending
f_b	Generalised external excitation force (N)
h_c	Length of the coil (m)
k	Preload spring stiffness coefficient (N/m)
m	Mass per unit length of each beam (kg/m)
m_s	Mass per unit length of the two beams together (kg/m)
n_s	Speed of the rotor housing the harvester (rpm)
q	Temporal generalised coordinate
r	eccentric radius (m)
$s_{a,i}, s_{b,i}$	Shape parameters of the beams' first mode shape for the i-th beam segment (m^{-1})
t_s	Thickness of the beams (m)
u_0	Axial displacement of the far-end support of the beams ($x_2 = 0$) (m)
$u_i(x_i, t)$	Axial displacement of the beams at x_i (m)
$\hat{u}_i(x_i, t)$	Axial displacement of the beams at x_i, with the same positive direction (m)
$w_i(x_i, t)$	Lateral displacement of the beams at x_i (m)
x_i	Distance of a point of the i-th beam segment (m)
Θ	Electromagnetic coupling factor (Vs/m)
Ω	Angular velocity of the rotor housing the harvester (rad/s)
β	Generalised nonlinear stiffness coefficient (N/m^3)
$\ddot{y}$	Base excitation (acceleration) of the housing rotor (rad/s^2)

$\delta(\cdot)$	Variational operator
$\delta_D(\cdot)$	Dirac-delta function
$\varepsilon_i(x_i, t)$	Strain of the beams at x_i
ρ	Density of the beams (kg/m^3)
$\sigma_{b,i}(x_i, t)$	Bending stress at point x_i (Pa)
$\varphi_i(x_i)$	First mode shape of the beams at point x_i (m)
ω	Frequency of torsional vibrations (rad/s)
$\omega_{n,c}$	First modal frequency of a cantilevered counterpart harvester (rad/s)
ω_n	First modal frequency of the harvester (rad/s)
A	Area of the beams' cross-section (m^2)

ACCEPTED MANUSCRIPT

1 INTRODUCTION

Vibration energy harvesting is a growing technological field that concerns scavenging energy from ambient mechanical vibrations and converting it to useful electricity [1] for the purpose of powering small electronic devices, such as sensors and wireless transmitters [2]. Usually, vibration energy harvesters are considered for applications where typical power mains are difficult to access such as structural health monitoring [3], tyre pressure monitoring systems [4] -[5] etc. Harvesting vibration energy allows remote powering of such distributed electronics.

The literature with proposed concepts and techniques for vibration energy harvesting is vast. Typically, a mechanical oscillator is coupled with an electroactive element, such as piezoelectric patches attached to a vibrating beam [6], or a coil of inductive wire in the proximity of a magnetic vibrating mass [7]. The oscillator is designed to resonate due to the vibrations of the host system, from which energy is to be harvested. However, the conditions for resonance are difficult to be met in a durable manner since ambient vibrations arising from environmental or mechanical loads are commonly subject to variations of their dominant frequency. This issue is particularly noteworthy when rotor machines with variable speed are considered for the host system, such as power transmission shafts. Variations of the rotor speed typically lead to corresponding variation of the dominant frequency of the host vibrations (torsional or translational). Therefore, vibration energy harvesters with set natural frequency (e.g. linear harvesters) are resonating only for a small fraction of the host's operating spectrum, leading the harvester to work off-tune with severe underperformance in terms of its power output.

This drawback is referred to as the bandwidth problem and it has concerned many recent research works. Among these, significant interest has been drawn by the proposed introduction of nonlinearity to the stiffness of the harvester [7], which results in a wider frequency range over which the oscillator vibrates with large amplitudes due to hardening/softening behaviour or due to other nonlinear phenomena, such as parametric resonance [8], bi-stability and multiple resonances [9]. The technique significantly relaxes the requirement for precise tuning of the harvester; however, large-scale frequency variations, as those typically observed in variable speed rotors, cannot be adequately answered since the response widening can only realistically cover a relatively narrow region around the linearized natural frequency. Even if essential nonlinearity is introduced, damping and restrictions imposed by the basin of attraction limit the efficient frequency range.

Instead, self-tuning tuning mechanisms have been proposed for such applications, which largely invoke the modification effect that an axial load has on the lateral frequency of a vibrating beam [10] –[12]. Tension or compression of a thin beam in its longitudinal direction is known to introduce a corresponding increase or decrease on the beam's modal frequencies respectively in the pre-buckling regime [13] -[14]. This property is particularly important for rotating systems with radially extending beam elements (rotor blades for instance), where inertial forces are always present. Bhat [15] calculated the modal frequencies of a rotating cantilever beam with a tip mass for increasing rotor speed and Naguleswaran [16] studied various combinations for the types of support of the beam's ends. Both works rigorously show the stiffening effect that increasing rotor speeds have on the lateral vibrations of a beam. Moreover, in the latter work, the selection of the axially restricted end was shown to have a distinct effect in the lateral frequency. In general, boundary conditions play an important role in determining the modal frequencies. Li [17] obtained analytical solutions for the transverse beam motion under generalised support forcing including axial loads. Further to that, Lenci and Rega [18] and Lenci et al. [19] considered the lateral dynamics with elastic support. They used an asymptotic approach to analyse a thin beam supported by a mechanical spring in the axial direction, showing that the spring stiffness may have a hardening or softening contribution to the beam overall stiffness, apart from frequency shifting due to preloads. These adjusting capabilities have been exploited by researchers for establishing self-tuning oscillations. Leland and Wright [11] proposed the use of axial load to appropriately adjust the resonant frequency of a piezoelectric bimorph harvester, largely introducing the technique for translational energy harvesting. Niri and Salamone [10] used a sliding mass connected to oblique springs with the resultant axial load tuning the frequency of a beam energy harvester, whereas Cheng et al. [12] used a piezoelectric actuator at one end of the beam in closed circuit with the vibrating parts, to passively control the axial load applied to the beam.

In rotor applications, centrifugal forces are utilized to establish self-tuning mechanisms for vibrating beams, due to their favourable dependence on the rotor speed. Gu and Livermore [20] first proposed exploiting this dependence to tune a radially extending cantilever with a tip mass and piezoelectric patches to the host rotational speed and they experimentally investigated the tuning effect. The stiffening effect was coupled with the frequency modification inherent in vibro-impact systems by the same authors [21], in an attempt to overcome the necessity for large root radius of the mounting support of the cantilever. Several modifications of this master design have been proposed in the literature primarily intended for spinning wheels [22] - [25] due to the relatively low rotational speeds of vehicle wheels. Elhadidi et al. [22] analysed a cantilever with magnetic tip coupled with an axially repulsive magnet that led to bi-stable potential energy. Wang et al. [23] introduced a tensile

preload to a trapezoidal cantilever's clamped support and Li et al. [24] introduced magnetoelectric transducers to effectively tune the harvester in low speeds further to the centrifugal stiffening effect. Hsu et al. [25] used a finite element approach to facilitate the master design of the cantilever harvester. The therein comprehensive analysis and experimental works demonstrated the self-tuning capabilities of a cantilever harvester alongside the concept's limitations. In particular, even if the tuning target is equal to the rotor speed ($1 \times n_s$), a large root radius is required to allow the harvester to be tuned to the slope of the rotating speed. From a physical point of view, the limitation is imposed by the lateral component of the centrifugal force that arises as soon as the cantilever tip starts vibrating. This component effectively acts as a negative virtual spring, as the analysis by Elhadidi et al. [22] clearly shows. A direct consequence is that the design becomes relatively insensitive to design modifications (e.g. tip mass weight) as the speed increases, practically disrupting the self-tuning concept. In other works, inverted cantilevered beams [26] have been considered, with additional magnetic coupling in pairs [27]. More advanced dynamics have also been investigated for vibration energy harvesting from rotational motion, including stochastic resonance that combines bi-stable dynamics with randomly fluctuating excitation profiles [28] [29] and even chaotic responses [30]. However, they are similarly subject to the limitations of the master cantilever concept.

In this paper, a novel self-tuned rotational vibration energy harvester is proposed consisting of an assembly of thin beams carrying a magnetic mass at an intermediate point and a tuning mass at their outer end. Such a layout has not been hitherto reported in the literature, offering the main advantage of a self-tuning mechanism which is insusceptible to the limitations pertinent to previous cantilevered designs. Vibration energy is converted to electrical via electromagnetic induction to a coil of wire. Section 2 introduces the proposed concept and the governing equations are extracted. The system's modal frequencies are obtained and the effect of the tensile tuning force on the beams' mode shapes is considered. The self-tuning mechanism is demonstrated in Section 3 using selected case studies of vibrations of up to $2 \times n_s$, which are further showcased in Section 4 (time history domain). The paper ends with a discussion of the main conclusions of this work.

2 THE PROPOSED ENERGY HARVESTER

The electromechanical system shown in Fig. 1 is considered. Two identical thin beams support a magnet of mass M_1. The beams are assumed to be made from a high strength material, such as blue tempered steel springs, and they have a uniform cross-section along their length L. The material's Young's modulus is denoted by E; ρ is its density, m is the

mass per unit length and I_s is the second moment of area of the cross-section. The rectangular cross-section has thickness denoted by t_s and width given by b_S, whereas it is assumed that is undergoes negligible shear deformations and thus it abides by the Euler-Bernoulli beam theory. The beams are clamped on one end to a rigid support rotating with angular velocity $\Omega = 2\pi n_s/60$, so that the whole assembly is free to rotate. The other end of the beams is clamped to a massless, undeformable rod that is free to slide along the beams' axial direction (or radial direction with respect to the rotating frame of reference). This rod also carries a weight M_2 at its midspan and it is connected to a linear spring with stiffness k, acting in the axial direction. Moreover, the two beams are connected by a massless, undeformable rod that spans perpendicularly to the beams' main axes, positioned at a distance L_1 from the clamped ends. A magnet of mass M_1 is attached on this rod, interacting with a coil of thin wire wrapped around the rod's longitudinal axis. The magnet's centre of mass is equally spaced between the two beams and the coil is positioned in such a way that the electromagnetic coupling is maximised, as it will be discussed later. The connecting rod also separates the beams into two segments, each point of which is at a distance x_i from its adjacent support for $i = 1, 2$, as shown in Fig. 1. Note that x_1 and x_2 are related by $x_2 = L - x_1$, leading to the definition $L_2 = L - L_1$. Opposite positive directions for x_1 and x_2 are chosen to ease the subsequent analysis following [31]. The distances L_1 and L_2 denote the same point on the beams with respect to the two beam segments, fulfilling continuity constraints.

Figure 1

2.1 Operating principle and main assumptions

The beams' assembly is allowed to vibrate in its transverse direction, as Fig. 1 shows. The relative motion between the magnet M_1 and the rigidly mounted coil induces voltage to the latter that can be harvested to power the electrical load R_L via the current flow of the closed circuit. The electromagnetic coupling is derived from solving the magnetic field and employing Faraday's law for a point magnet and then using a correction factor for ring magnets. In fact, following Owens and Mann [32] and referring to Fig. 2, the voltage V_c induced to the coil is given by:

$$V_c = \Theta\big(w_1(L_1)\big)\, \dot{w}_1(L_1) \tag{1}$$

where $\Theta\big(w_1(L_1)\big)$ is the electromechanical coupling factor given by:

$$\Theta\big(w_1(L_1)\big) = \frac{N_c B_r \rho_s M_1 \xi}{2A_c} \sum_{i,j=1}^{2} (-1)^{i+j} \left[\ln(r_i + Z_{ij}) - \frac{r_i}{Z_{ij}} \right] \tag{2}$$

with $Z_{ij}^2 = r_i^2 + \big[z_j - w_1(L_1)\big]^2$ and $A_c = (r_2 - r_1)(z_2 - z_1)$ (with dimensions shown in Fig. 2); N_c is the number of coil turns, B_r is the remnant magnetic field intensity, ρ_s is the magnet density and ξ is the coil fill factor, which is a ratio of the conductive material's volume over the total coil volume including the wire coating. Hence, the current flowing in the closed circuit is derived through Kirchoff's second law and is coupled to the mechanical response of the beam assembly via $\Theta(z)$ and $\dot{w}_1(L_1)$.

Figure 2

Since the beams are identical and symmetrically placed, the undeformable connecting rod allows the assumption that the beams vibrate with equal lateral displacements and velocities, i.e. $w_i(x_i, t) = w_i^*(x_i, t)$ and $u_i(x_i, t) = u_i^*(x_i, t)$ for $i = 1, 2$. In what follows, the asterisk is omitted from the notation for simplicity, as well as the functional arguments except when it is required otherwise (e.g. for $x_1 = L_1$). Moreover, the axial rigidity of the thin beams, EA, is much larger than their flexural rigidity, EI. The rotary displacement of the magnet M_1 with respect to each of the beams is supressed by the axial stiffness of the symmetrically positioned beams and therefore, the rotary inertia of the magnet can be ignored as far as bending motion is considered. If the connecting rod was deformable, this would hold true only for $L_1 = L/2$. However, the rigidity of the connecting rod leads to negligible inertia for any $L_1 \in (0, L)$. Moreover, we can assume that the connecting rod is clamped onto the beams at L_1. Therefore, the geometry of the assembly constrains the beams to have zero slopes at the points attached to the connecting rod, i.e. $\dot{w}_1(L_1, t) = \dot{w}_2(L_2, t) = 0$. This assumption will be useful for simplifying the system's boundary conditions and the mathematical derivations relevant to the natural frequency equations.

The beams considered in this paper are thin, i.e. $t_s \ll L$, and consequently the local strain ε of a beam element follows the linear Euler-Bernoulli beam theory (where ´ denotes derivative with respect to spatial coordinate):

$$\varepsilon_i = \sqrt{(1+\hat{u}_i')^2 + w_i'^2} - 1 + z\,\frac{(1+\hat{u}_i')w_i'' - \hat{u}_i''w_i'}{\left[(1+\hat{u}_i')^2 + w_i'^2\right]^{3/2}} \tag{3}$$

where $\hat{u}_i(x_i,t) = (-1)^{i-1}u_i(x_i,t)$ to account for the change of positive direction of the axial displacement in the two i segments. The first two terms of the RHS correspond to strain due to axial deformation, denoted by e_0, whereas the last term corresponds to strain from bending, e_b, with z denoting the distance of a point in the cross-section from the beam midplane axis along the t_s thin dimension. Considering that one end of each beam is free to move along the axial direction and that $EA \gg EI$ and $EA \gg kL$, we may impose the inextensionality condition that leads to:

$$e_0 = 0 \Rightarrow \sqrt{(1+\hat{u}_i')^2 + w_i'^2} - 1 = 0 \tag{4}$$

Essentially, Eq. (4) means that any axial displacement $\hat{u}_i$ is induced only by the transverse motion w_i. If this condition is relaxed, the beams can undergo stretching, which is known to incur strong nonlinearities in the dynamics of the problem [13]. However, this phenomenon would require fixed ends to unfold, or at least a resistive support stiffness comparable to the beam's axial one. Herein, by assuming that $EA \gg kL$, stretching can be shown to be of very small magnitude. We may thereby solve Eq. (4) for the axial slope to arrive at:

$$\hat{u}_i' = \sqrt{1 - w_i'^2} - 1 \tag{5}$$

where the boundary conditions of the undeformed beam have been taken into account. Expanding to a Taylor series up to 4-th order we get:

$$\hat{u}_i' = -\frac{1}{2}\left(w_i'^2 + \frac{1}{4}w_i'^4\right) \tag{6}$$

Upon integration of Eq. (6), each segment's end displacement can be obtained and the total end shortening of the whole assembly of the beams is derived as:

$$\hat{u}_1(L) = \hat{u}_2(0) = -\sum_{i=1}^{2} \frac{1}{2} \int_0^{L_i} \left(w_i'^2 + \frac{1}{4} w_i'^4 \right) dx_i \tag{7}$$

Furthermore, the beams' strain is solely dependent on the bending strain, which upon expansion up to 4-th order becomes:

$$\varepsilon_i = z \left(w_i'' + \frac{1}{2} w_i'' w_i'^2 \right) \tag{8}$$

Equations (3)-(8) will be recalled in the next section for the derivation of the governing equations.

The harvester assembly is attached to a rotating inertial frame that exerts centrifugal forces on the beam and the lumped masses. Coriolis forces are also acting in the radial direction due to the beams' transverse vibrations; yet, their magnitude can be considered small enough to be neglected, especially for relatively high rotational speeds when the centrifugal force can be orders of magnitude bigger than the Coriolis force due to its dependence on Ω^2 instead of Ω. In what follows, we shall only consider the effect of the rotational inertial framework due to the lumped masses, assuming that $M_i \gg 2mL$, $i = 1, 2$.

The beam assembly carries two lumped masses: one at an arbitrary point $x_i = L_i$ and another at the moveable end $x_2 = 0$. The centrifugal forces acting on theses masses apply tension to the beam proportional to Ω^2 and subject to the mass weight and location. The axial forces applied on a beam in transverse vibration mode are known to provide a frequency altering effect, either stiffening (tensile load) or softening (compressive load) that can even lead to buckling [13]. This allows the possibility to design a beam assembly, where the natural frequencies are knowingly changing with variations of the rotational speed. In most rotational engineering applications, the main frequency of torsional vibrations of shafts and other components is typically a multiple of the rotational speed (e.g. automotive, marine, aerospace applications). Careful manipulation of the design such that the natural frequency variation corresponds to the main (fluctuating) vibration frequency, could lead the system to operate in resonance as long as this relation holds. The assembly design is

also complemented with an axial compressive force due to the elastic support k, which is included to allow farther flexibility in the design. Potentially, a passive tuning design strategy is established with favourable results for vibration energy harvesting. The advantage of the proposed concept is due to the positioning radius of the harvester. Previous literature regarded devices that needed a considerable offset radius to achieve tuning of the beam-based harvesters. Effectively, this drawback limited the range of the potential applications to rotors working at relatively low speeds. The herein proposed concept offers the possibility of tuning at high working speeds, taking into account more accurate expressions of the system's mode shapes that may influence the practical implementation of the designed tuning.

2.2 Governing equations

We shall employ Hamilton's extended principle to extract the governing equations, which requires the extraction of the system Lagrangian $\mathcal{L} = T - U$, where T is the kinetic energy and U is the potential energy, complemented by the work done by non-conservative forces W^{nc}. The kinetic energy of the system is given by:

$$T = \frac{1}{2}\sum_{i=1}^{2}\left\{\int_0^{L_i} m\left(\dot{w}_i^2 + \dot{\hat{u}}_i^2\right)dx_i + \int_0^{L_i} m\left(\dot{w}_i^{*2} + \dot{\hat{u}}_i^{*2}\right)dx_i\right\} + \frac{1}{2}M_1\left[\dot{w}_1^2(L_1) + \dot{\hat{u}}_1^2(L_1)\right] + \frac{1}{2}M_2\dot{\hat{u}}_2^2(0) \tag{9}$$

where the last two terms correspond to the kinetic energy of the masses M_1 and M_2 in transverse and axial directions. Recalling that the beams are identical, Eq. (9) becomes:

$$T = \frac{1}{2}\sum_{i=1}^{2}\left\{\int_0^{L_i} m_s\,\dot{w}_i^2 dx_i\right\} + \frac{1}{2}M_1[\dot{w}_1^2(L_1)] \tag{10}$$

where $m_s = 2m$. In this paper, nonlinear inertia is not considered since it does not contribute to the sought tuning mechanism and so, the axial velocities $\dot{\hat{u}}_i$ are neglected from the expression of the kinetic energy. Then, recalling that the beams are identical, the potential energy reads:

$$U = \frac{1}{2}\sum_{i=1}^{2}\left[\int_0^{V_i} 2\sigma_{b,i}\,\varepsilon_{b,i}dV_i - \int_{\hat{u}_i(0)}^{\hat{u}_i(L_i)} P_i\,d\hat{u}_i\right] + \frac{1}{2}k[u_0 + \hat{u}_2(0)]^2 - \frac{1}{2L_1}\int_0^{L_1}\delta_D(x_1 - L_1)P_{M_1}w_1^2(x_1)\,dx_1 \tag{11}$$

where u_0 is an initial compression of the spring k responsible for pre-loading the system and $\delta_D(\cdot)$ is the Dirac delta function. The axial load P is defined across the span of the beams and it is given by:

$$P = \begin{cases} P_1 = P_{M_1} + P_{M_2}, & 0 < x_1 < L_1 \\ P_2 = P_{M_2}, & 0 < x_2 < L_2 \end{cases} \tag{12}$$

where $P_{M_1} = M_1\Omega^2 L_1$ and $P_{M_2} = M_2\Omega^2 L$ are the centrifugal forces acting on the lumped masses and tensile loads are taken positive. The material has been assumed to obey the linear stress-strain relationship, $\sigma_{b,i} = E\varepsilon_{b,i}$. Substituting this equation for the stress, the strain expression from Eq. (8), defining $E_s = 2E$, substituting $d\hat{u}_i$ using Eq. (6) and Eq. (7) and recalling that $\hat{u}_2 = -u_2$, Eq. (11) up to 4-th order becomes:

$$U = \frac{1}{2}\sum_{i=1}^{2}\int_0^{L_i}\left[E_s I_s\left(w_i''^2 + w_i''^2 w_i'^2\right) + \frac{P_i}{2}\left(w_i'^2 + \frac{1}{4}w_i'^4\right)\right]dx_i + \frac{1}{2}k\left[u_0 - \sum_{i=1}^{2}\frac{1}{2}\int_0^{L_i}\left(w_i'^2 + \frac{1}{4}w_i'^4\right)dx_i\right]^2 - \frac{1}{2}\frac{P_{M_1}}{L_1}w_1^2(L_1) \tag{13}$$

The work of non-conservative forces comprises external and damping forces:

$$W_i^{nc} = \sum_{i=1}^{2}\int_0^{L_i} F(t)\,w_i\,dx_i - \sum_{i=1}^{2}\int_0^{L_i} c\dot{w}_i\,w_i\,dx_i \tag{14}$$

$F(t)$ is an externally applied force and c is the structural viscous damping coefficient. We may hereby apply the extended Hamilton's principle:

$$\mathcal{H} = \int_{t_1}^{t_2} \delta T - \delta U + \delta W^{nc} = 0 \tag{15}$$

where $\delta(\cdot)$ is the variational operator. This leads to the following equation of motion for the i–th beam segment:

$$\begin{aligned} m_s\ddot{w}_i + c\dot{w}_i + E_sI_s\left(w_i'''' + w_i'''' {w_i'}^2 + w_i' {w_i''}^2\right)' - P_i\left(w_i'' + \frac{3}{2}{w_i'}^2 w_i''\right) \\ + k\left(w_i'' + \frac{3}{2}{w_i'}^2 w_i''\right)\left[u_0 - \sum_{i=1}^{2}\frac{1}{2}\int_0^{L_i}\left({w_i'}^2 + \frac{1}{4}{w_i'}^4\right)dx_i\right] = F(t) \end{aligned} \tag{16}$$

and the corresponding boundary conditions (coupled via continuity constraints at $x_1 = L_1$):

$$\begin{aligned} x_1 = 0: &\quad w_1(0) = w_1'(0) = 0 \\ x_1 = L_1 \text{ and } x_2 = L_2: &\quad \begin{aligned} &w_1'(L_1) = w_2'(L_2) = 0 \\ &w_1(L_1) = w_2(L_2) \\ &M_1\ddot{w}_1(L_1) = E_sI_s[w_1'''(L_1) + w_2'''(L_2)] + \frac{P_{M_1}}{L_1}w_1(L_1) \end{aligned} \\ x_2 = 0: &\quad w_2(0) = w_2'(0) = 0 \end{aligned} \tag{17}$$

Equations (16) and (17) describe the spatiotemporal response of the harvester for open circuit. For a closed circuit the system of equations is complemented by Kirchoff's 2nd law and the additional electromagnetic dissipation of the mechanical response:

$$m_s\ddot{w}_i + c\dot{w}_i - \delta_D(x_1 - L_1)\Theta[w_1(L_1)]I + E_sI_s\left(w_i''' + w_i'''w_i'^2 + w_i'w_i''^2\right)' - P_i\left(w_i'' + \frac{3}{2}w_i'^2w_i''\right) + k\left(w_i'' + \frac{3}{2}w_i'^2w_i''\right)\left[u_0 - \sum_{i=1}^{2}\frac{1}{2}\int_0^{L_i}\left(w_i'^2 + \frac{1}{4}w_i'^4\right)dx_i\right] = F(t) \quad (18)$$

$$L_H\dot{I} + (R_c + R_L)I + \Theta[w_1(L_1)]\dot{w}_1(L_1) = 0$$

Note that the electromagnetic damping applies only to the $i = 1$ segment and the Dirac-delta function concentrates its action at the position of the vibrating magnet, $x_1 = L_1$.

2.3 Modal frequencies and mode shapes

The performance of the proposed design relies on the effective tuning of its natural frequency to the expected frequency range of the host vibrations. It is therefore paramount to quantify the variation of the first modal frequency of the assembly and the corresponding mode shape with rotational speed variation. The harvester is divided into two segments, coupled by continuity constraints at $x = L_1$. Equations (17) and (18) are linearised and solved separately to acquire the frequency equations. Superimposing the boundary conditions and the continuity constraint leads to a single frequency equation, which is solved numerically. Linearising Eq. (18) and neglecting non-conservative work leads to:

$$m_s\ddot{w}_i + E_sI_sw_i'''' - P_iw_i'' + ku_0w_i'' = 0, \qquad i = 1,2 \quad (19)$$

We shall consider only the first mode of the beam and thus $w_i(x_i, t) = \phi_i(x_i)q(t)$ may be assumed, whereas $\ddot{q} = -\omega_n^2 q$ (see [14] for instance). Then, Eq. (19) becomes:

$$E_sI_s\varphi_i'''' - (P_i - ku_0)\varphi_i'' - m_s\omega_n^2\varphi_i = 0, \qquad i = 1,2 \quad (20)$$

The above differential equation accepts solutions of the following form:

$$\varphi_i(x_i) = A_i \cos s_{a,i}x_i + B_i \cosh s_{b,i}x_i + C_i \sin s_{a,i}x_i + D_i \sinh s_{b,i}x_i\,, \qquad i = 1{,}2 \quad (21)$$

where $s_{a,i}$ and $s_{b,i}$ are parameters given by:

$$\begin{aligned} s_{a,i} &= \sqrt{\frac{-P_i + \sqrt{4E_sI_sm_s\omega_n^2 + P_i^2}}{2E_sI_s}}, \qquad i = 1{,}2 \\ s_{b,i} &= \sqrt{\frac{P_i + \sqrt{4E_sI_sm_s\omega_n^2 + P_i^2}}{2E_sI_s}}, \qquad i = 1{,}2 \end{aligned} \quad (22)$$

Utilizing the boundary conditions at $x_1 = 0$ and $x_2 = 0$, Eq. (21) becomes:

$$\varphi_i(x_i) = A_i(\cos s_{a,i}x_i - \cosh s_{b,i}x_i) + C_i(\sin s_{a,i}x_i - \sinh s_{b,i}x_i), \qquad i = 1{,}2 \quad (23)$$

and the continuity constraint: $w_1'(L_1) = w_2'(L_2) = 0$, further simplifies this expression with:

$$C_i = \frac{A_i(s_{a,i}\sin s_{a,i}L_i + s_{b,i}\sinh s_{a,i}L_i)}{s_{a,i}(\cos s_{a,i}L_i - \cosh s_{a,i}L_i)}, \qquad i = 1{,}2 \quad (24)$$

Using the first mode generalised response, the remaining boundary condition that regards forces in the transverse direction becomes:

$$M_1\omega_n^2\varphi_1(L_1) + E_sI_s[\varphi_1'''(L_1) + \varphi_2'''(L_2)] + \frac{P_{M_1}}{L_1}\varphi_1(L_1) = 0 \quad (25)$$

Substituting Eq. (22)–(24) into Eq. (25) and into the continuity constraint for the deflection at $x_1 = L_1$: $\varphi_1(L_1) = \varphi_2(L_2)$, leads to a 2×2 linear matrix equation with respect to $A_i, i = 1, 2$. The matrix equation has non-trivial solutions only when the 2×2 coefficient

matrix has a non-zero determinant, which is the final equation with respect to ω_n that is numerically solved to compute the first modal frequency. Afterwards, the unknown coefficients A_i are computed by imposing the normalisation condition on top of the deflection continuity constraint at $x_1 = L_1$: $\varphi_1(L_1) = \varphi_2(L_2)$.

$$\int_0^{L_1} m_s \varphi_1^2 \, dx_1 + \int_0^{L_2} m_s \varphi_2^2 \, dx_2 + M_1 \varphi_1^2(L_1) = 1 \tag{26}$$

The analysis so far has allowed an accurate estimation of the influence of the different axial loads that the two segments of the beams are exposed to. Moreover, the vibrating magnet can be positioned at an arbitrary point x_1, which additionally influences the mode shapes of the assembly. Previous literature has hitherto disregarded the effect of the changing mode shapes, which can potentially lead to significant errors when the rotational speeds are relatively high. Fast rotations lead to parabolically increasing axial forces that determine the mode shapes to a great extent and consequently, the modal frequencies. A case study is considered to show the mode shape variation with respect to the rotational speed of the assembly. The assumed parameters are listed in Table 1.

Parameter	Value
E_s	400 GPa
b_s	0.02 m
t_s	203 10^6 m
ρ	7810 kg/m^3
L	0.075 m
L_1	0.04 m
M_1	0.108 kg
M_2	0.0243 kg
k	8.942 10^3 N/m

u_0	0.00313 m

Table 1. Parameters considered in the numerical case study.

Fig. 3 shows the first mode shape for static conditions and three rotational speeds: 1800, 3600 and 6000 rpm. Clearly, there is a distinguished variation of the mode shape when the rotational speed is increasing. The effect of this variation is even more substantial when calculating the modal frequency (with participation of the first and second spatial partial derivatives of the mode shape):

$$\omega_n^2 = \int_0^{L_1} \left[E_s I_s \varphi_1''^2 + (P_1 - k u_0)\varphi_1'^2\right] dx_1 + \int_0^{L_2} \left[E_s I_s \varphi_2''^2 + (P_2 - k u_0)\varphi_2'^2\right] dx_2 - \frac{P_{M_1}}{L_1}\varphi_1^2(L_1) \quad (27)$$

Figure 3

Neglecting the dependence of mode shapes on the rotational speed can lead to miscalculation of the modal frequency when fast rotations are considered. Past literature has largely neglected the effect of varying mode shapes onto potential tuning mechanisms. Usually, a trial function [22],[27] or a constant mode shape [20],[21],[25] was chosen to represent the mode shape of a thin beam for all rotational speeds. Therefore, the magnified influence of the axially acting centrifugal forces on a fast rotating beam, have been misrepresented in previous models. To highlight the importance of accurately including the expressions for the mode shapes, the herein described procedure for computing the system's modes is applied to the previous case study and the resultant modal frequency is compared against the result of a simplified approach. The simplified approach assumes that the mode shape of the beam is fixed for all rotational speeds (equal to the static mode shape of zero rotational velocity). Thus, the frequency is computed by changing the magnitude of the axial force only.

Figure 4

Fig. 4 shows that when the host rotor runs at relatively high speeds the variation of the mode shapes should be accounted for. Even though the error does not exceed 10%, one

should consider that self-tuned harvesters normally operate based on maintaining linear resonance over the tunable range. Overestimation of the harvester's natural frequency by the observed error may lead to substantial frequency mismatch and to severe reduction of the extractable electrical power when linear resonance is sought. Therefore, it is shown that accurate expressions for the mode shapes should be used for high rotational speeds.

3 SELF-TUNING

The harvester is self-tuned such that the first modal frequency follows the expected vibration frequency along a range of rotational speeds. Normally, the frequency of torsional vibrations in rotating systems is proportional to the rotational speed. For example, 4-cylinder IC engines generate (predominantly) 2nd order torsional oscillations on the vehicle's powertrain. In this scenario, one would aim at designing the harvester such that its modal frequency is twice the rotational speed.

The modal characteristics of the herein proposed harvester depend on typical parameters for Euler-Bernoulli beams, such as the geometry (b_s, t_s, L) and material properties (ρ, E_s, I_s). Additionally, the axial forces that tune the assembly's frequency depend on the position and weight of the vibrating magnet, L_1, M_1, that of the far-end mass, L, M_2, and on the preload, $P_{pre} = ku_0$. In given applications, the total lumped mass, $M_t = M_1 + M_2$, and the assembly size are usually dictated by collateral constraints. Hence, the analysis would be more interesting with respect to non-dimensional parameters. In this section, parametric studies are conducted on the distribution of mass, M_1/M_t, on the relative positioning of the magnet, L_1/L, and on the magnitude of the preload, P_{pre}, to show the variation of the tuning mechanism and the consequent design options.

The above parameters are varied independently from each other in Fig. 5 – Fig. 7, and the resulting variation of the modal frequency is plotted. The presented graphs are generated for the parameters of Table 1, except for the independently varied parameter on each graph. Fig. 5 depicts the variation of the modal frequency with changing the distribution of mass. At relatively low speeds, frequencies undergo a minor adjustment; however, at higher speeds where the axial centrifugal forces are stronger, the curve is substantially varied in an almost linear fashion. Concentrating mass at the far end of the beams leads to a higher slope of the frequency curve. This is due to the higher intensity of the centrifugal force that acts on M_2, as opposed to M_1. Comparing the variation of the slope in Fig. 5 with that in Fig. 6 and Fig. 7, we note that the distribution of mass is much more effective than the position of M_1 or the preload in adjusting the slope of the frequency curve. Therefore, the first step

in tuning the harvester to the identified order of vibrations (1x, 2x the rotational speed) is to adjust the distribution of mass such that the slope of the modal frequency curve approaches the slope of the torsional vibrations frequency. On the other hand, changing the position of the magnet, shown in Fig. 6, leaves the slope unaffected. Nevertheless, L_1/L introduces an almost uniform offset of the curve along the vertical axis. This attribute can be used to move the curve to the desired frequency values without mistuning the slope of the curve.

Figure 5

Figure 6

Finally, the influence of applying a compressive preload at the far-end of the beams ($x_2 = 0$) is considered in Fig. 7. Note that when the harvester is not rotating ($n_s = 0$) the applied load may lead to buckling of the beams, if the preload is greater than the critical buckling load. As a matter of fact, the last case in Fig. 7 (P_{pre} =80 N) corresponds to a buckled harvester. This is why the depicted frequency curve has its origin just after 800 rpm. Of course, buckled beams can be also subject to oscillatory response, but the slope of the curve in the buckled range would be negative and, as such, of no use for the herein considerations. Besides, several rotor applications operate over a minimum speed (e.g. internal combustion engines work above the idling speed). The preload is more prominent in the lower speed range, where the mass distribution could not have a strong influence. At the same time, both the curve slope and the modal frequency values at the higher speed range are almost unaffected by the preload. Therefore, the applied preload can be used as the third step in tuning the harvester at lower speeds, where the previously examined parameters were unable of doing so.

Figure 7

3.1 Case studies

The above presented procedure for designing the harvester such that its modal frequency is passively tuned to the frequency of vibrations is demonstrated. In rotor applications, torsional vibrations are typically manifested at multiples of the main rotor speed. In this section, three case studies are considered for the dominant order of the vibrations using the

parameters of Table 2; namely, $1\times$, $1.5\times$ and $2\times$ the rotational speed (n_s). The first modal frequency is computed across a wide range of operating speeds (0 - 6000 rpm) and it is compared against the frequency of the vibrations. Ideally, the two curves shown in each of Fig. 8 - Fig. 10 should coincide to achieve perfect self-tuning. Even though not strictly necessary, the total mass of the tuning elements (M_t) is kept constant for all three case studies. This is to demonstrate the flexibility of the design to target different orders of vibration frequencies via minor configuration adjustments of the mass distribution, the vibrating magnet position and the applied preload. A comprehensive parameter optimisation process might well lead to successful self-tuning.

Parameter	**Value**
E_s	400 GPa
b_s	0.02 m
t_s	203 10^6 µm
ρ	7810 kg/m^3
L	0.058 m
M_t	0.182 kg
k	8.942 10^3 N/m
B_r	1.31 T
L_H	75.6 10^{-3} H
R_c	93 Ohms
R_L	100 Ohms
h_c	0.015 m
D_o	0.045 m
D_i	0.036 m
N_c	1300 turns

$M_{1,nm}$	0.029 kg

Table 2. Parameters considered in the numerical case studies shown in Fig. 8 – Fig. 10.

Fig. 8 shows the results for the first case study that considers $1 \times n_s$ rotational vibrations. The slope of the vibrations frequency with increasing n_s is relatively gentle and so, following the parametric analysis in Fig. 5, most of the mass is kept with the vibrating magnet ($M_1/M_t = 81.86\%$). Furthermore, the magnet is positioned exactly at the midspan of the beams to offset the self-tuned modal frequency to the lowest possible range. Last, a considerable preload is applied, yet lower than the critical buckling load, to adjust the lower speed range. Note that the slopes of the two curves in Fig. 8 are almost equal, which is the envisaged target. Since the modal frequency increases with a rate similar to the excitation frequency, the same response amplitude can be maintained across the examined frequency range. Therefore, resonant or near-resonance response can be sustained for any operational speed within the considered limits, leading to broadband energy harvesting.

Figure 8

Figure 9

A similar procedure can be applied for $1.5 \times n_s$ and $2 \times n_s$ vibrations, as shown in Fig. 9 and Fig. 10. The computed frequencies in Fig. 9 have simia lar pattern with the previous results in Fig. 8. The slope of the vibrations frequency is steeper and therefore, the mass is distributed more evenly ($M_1/M_t = 65.93\%$), but the position of the magnet is the same as before, whereas the preload has slightly been increased to 62N. Fig. 10, however, exhibits a qualitatively different picture. A steeper slope ($2 \times n_s$) requires more inertia placed at the far-end of the beams ($M_1/M_t = 52.19\%$), and the preload has been increased to 85 N, which is higher than the critical buckling load. Therefore, at low speeds including the static case the beams are buckled. As the rotational speed increases, higher centrifugal loads are exerted onto the system and consequently, the beams return to a pre-buckling shape above 900 rpm. We note that the achieved self-tuning in Fig. 10 is almost ideal, since the modal frequency almost coincides with the excitation frequency for the examined speed range.

Figure 10

4 NUMERICAL CASE STUDIES

The time history of the system's mechanical response and electrical output can be computed by solving the equation of motion (18). Assuming that the response is dominated by the first mode, $w_i = \varphi_i(x_i)q(t)$, multiplying by $\varphi_i(x_i)$ and integrating over each segment's domain, the differential equation for each segment becomes:

$$\begin{aligned}\int_0^{L_i} m_s\varphi_i^2\,dx_i\,\ddot{q} &+ \int_0^{L_i} c\varphi_i^2\,dx_i\,\dot{q} - \int_0^{L_i} \delta_D(x_1 - L_1)\varphi_i\Theta[\varphi_1(L_1)q]I\;dx_i \\ &+ \int_0^{L_i} [E_sI_s\varphi_i\varphi_i'''' - (P_i - ku_0)\varphi_i\varphi_i'']\,dx_i\,q \\ &+ \int_0^{L_i}\left[E_sI_s\varphi_i\left(\varphi_i'''\varphi_i'^2 + \varphi_i'\varphi_i''^2\right)' - \frac{3}{2}(P_i - ku_0)\varphi_i\varphi_i'^2\varphi_i''\right. \\ &\left. - k\varphi_i\varphi_i''\sum_{i=1}^{2}\frac{1}{2}\int_0^{L_i}\varphi_i'^2\,dx_i\right]dx_i\,q^3 = \int_0^{L_i}\varphi_iF(t)\,dx_i, i = 1{,}2\end{aligned} \tag{28}$$

$$L_H\dot{I} + (R_c + R_L)I + \Theta[\varphi_1(L_1)q]\varphi_1(L_1)\dot{q} = 0$$

Applying integration by parts where applicable leads to:

$$\begin{aligned}\int_0^{L_i} m_s\varphi_i^2\,dx_i\,\ddot{q} &+ \int_0^{L_i} c\varphi_i^2\,dx_i\,\dot{q} - \int_0^{L_i} \delta_D(x_1 - L_1)\varphi_i\Theta[\varphi_1(L_1)q]I\;dx_i \\ &+ \int_0^{L_i} \left[E_sI_s\varphi_i''^2 - (P_i - ku_0)\varphi_i'^2\right]dx_i\,q \\ &+ \int_0^{L_i}\left[2E_sI_s\varphi_i'^2\varphi_i''^2 + \frac{1}{2}(P_i - ku_0)\varphi_i'^4\right. \\ &\left. + k\varphi_i'^2\sum_{i=1}^{2}\frac{1}{2}\int_0^{L_i}\varphi_i'^2\,dx_i\right]dx_i\,q^3 = \int_0^{L_i}\varphi_iF(t)\,dx_i\end{aligned} \tag{29}$$

$$L_H\dot{I} + (R_c + R_L)I + \Theta[\varphi_1(L_1)q]\varphi_1(L_1)\dot{q} = 0$$

Adding the equations for the two segments, $i = 1, 2$ and utilizing the normalisation condition (26) and the frequency equation (27), the equation of motion in generalised coordinates becomes:

$$\ddot{q} + c_b\,\dot{q} - \varphi_1(L_1)\Theta[\varphi_1(L_1)q]I + \omega_n^2 q + \beta q^3 = f_b$$
$$L_H\dot{I} + (R_c + R_L)I + \Theta[\varphi_1(L_1)q]\varphi_1(L_1)\dot{q} = 0 \tag{30}$$

where

$$c_b = \sum_{i=1}^{2}\int_0^{L_i} c\varphi_i^2\,dx_i$$
$$\beta = \sum_{i=1}^{2}\int_0^{L_i}\left[2E_sI_s\varphi_i'^2\varphi_i''^2 + \frac{1}{2}(P_i - ku_0)\varphi_i'^4 + k\varphi_i'^2\sum_{i=1}^{2}\frac{1}{2}\int_0^{L_i}\varphi_i'^2\,dx_i\right] \tag{31}$$
$$f_b = \sum_{i=1}^{2}\int_0^{L_i}\varphi_i F(t)\,dx_i$$

Note that the response of the harvester will also be subject to the effect of the nonlinear stiffness coefficient, β. It is assumed that the harvester is to be used as an attachment to a larger host structure. Therefore, the type of forcing that the harvester will be subject to can reasonably be assumed as a base excitation ($\ddot{z}$ is the input vibrations of the mounting shaft):

$$f_b = \ddot{\gamma}\left[M_1\varphi_1(L_1) + \sum_{i=1}^{2}\int_0^{L_i}\varphi_i m_s\,dx_i\right] \tag{32}$$

The case studies of the previous section for the vibrations of the three different speed orders are extended with computation of the response time history, via Runge-Kutta numerical integration of Eq. (30) – (32). The analysis is focused on the magnet's transverse velocity and on the voltage generated. Moreover, the corresponding time history of the power output is shown, as well as the axial displacement of the far-end support to confirm its negligible magnitude. The parameters used in the simulations for the beams, the masses and the coil are shown in Table 2, whereas the tuning parameters are varying as in Section 3. It is assumed that M_1 is not fully magnetic, but rather an assembly of magnets with non-magnetic mounting parts with mass $M_{1,nm}$.

The time histories presented in Fig. 11 – Fig. 13 verify the expected broadband character of the harvester's output. In all case studies, the magnet's velocity retains almost constant amplitudes for all the examined speeds. This is also consistent with the voltage induced at

the closed circuit ends of the coil, which also demonstrates a relative insensitivity to the rotor speed. It is also noted that the axial displacement of the harvester remains at considerably low values (below 0.6 mm for all cases), which validates the initial assumption of negligible nonlinear inertia. The results of Fig. 13 also show that when the modal frequency curves from Section 3 (Fig. 8 - Fig. 10) cross the examined vibrations frequency curve, an increase of the output is observed that corresponds to perfect resonance. This is observed in all the time histories in Fig. 13 at about 1800 rpm. Cross-correlating with Fig. 10, it is verified that this resonance occurs due to the perfect match of the tuned frequency to the instantaneous vibration frequency. Nevertheless, in this case as well, the amplitudes of the voltage output and the corresponding power delivered to the load are retained within a considerable range. For example, the voltage output in Fig. 13(b) is above 2.5 V for every speed above 1500 rpm. This corresponds to significantly broad response spectrum of about 75 Hz. Effectively the proposed harvester can operate without the known bandwidth limitations that linear and, to some extent, nonlinear energy harvesters suffer from. The numerical results have demonstrated the capability of establishing nearly purely broadband output.

Figure 11

Figure 12

Figure 13

4.1 Comparison against a cantilever beam harvester

The proposed concept for harvesting energy from torsional vibrations was shown to offer a substantial degree of flexibility for self-tuning to the dominant frequency of oscillations. More importantly, the concept promises effective tuning for a wide speed range of the housing rotor, including relatively high speeds. This is a noteworthy step forward for rotational vibration energy harvesting. In particular, the majority of existing self-tuned harvesters have been following the generic layout of a cantilever beam with a tip mass, utilizing axial gyroscopic forces acting on the tip mass to introduce self-tuning. Here, the performance of the proposed harvester for the case of $1 \times n_s$ vibrations will be compared

against a variety of cantilever beam designs to demonstrate its potential to improve the performance of existing self-tuned harvesters.

The cantilever beam counterpart follows similar dynamics with the proposed harvester, with a few – yet crucial – differences. It is modelled using clamped-free boundary conditions instead of the hybrid boundary conditions shown in Fig. 1. Moreover, the mass is concentrated at the tip of the harvester. The self-tuning mechanism of the cantilever harvester can be adjusted by varying the tip mass weight and the cantilever length, both intended to alter the magnitude of centrifugal forces in order to induce an appropriate slope to the modal frequency curve. The axial force can also be adjusted by offsetting the root of the beam to a radius r, even though this may have an adverse impact on the size of the device and the required installation space. Therefore, a similar analysis can be applied using only the $i = 1$ segment of the beams and modifying the boundary conditions in Eq. (17) accordingly, leading to a modified version of Eq. (27), where k is omitted and mode shape φ_1 corresponds to that of a cantilever beam:

$$\omega_{n,c}^2 = \int_0^{L_1} \left[E_s I_s \varphi_1''^2 + P_{M_1} \varphi_1'^2 \right] dx_1 - \frac{P_{M_1}}{L_1} \varphi_1^2(L_1) \tag{33}$$

For the purpose of comparing the tuning capability of the two concepts the total size of the examined case studies is kept equal, $L = 0.058$ m. When the cantilever length L_1 is varied, the difference with respect to L is introduced as offset, $r = L - L_1$. Fig. 14 and Fig. 15 show the frequency curve of the proposed harvester as taken from Fig. 8, along with the considered frequency of oscillations at $1 \times n_s$. These curves are compared against $\omega_{n,c}$ for selected variations of the cantilever beam harvester. In particular, the cases shown in Fig. 14 correspond to $M_1 = 0.182$ kg and varying L_1, whereas the curves of Fig. 15 are calculated for L_1=0.018 m and varying M_1. It is evident from both figures that the cantilever beam harvester is limited on the slope that its modal frequency can follow with increasing speed, which results to reduced capability in adjusting the modal frequency of the harvester to the frequency of oscillations. On the other hand, the proposed concept can tune itself almost to an ideal frequency match regardless of the magnitude of the rotational speed, subject to the necessary optimisation.

Figure 14

Figure 15

The restrictions in the performance of the cantilever beam harvester are fundamentally related to Eq. (33) and specifically to the second term of its right-hand-side. The first term in the integrand controls the constant part of the cantilever's modal frequency and the passive tuning is achieved by the combination of the second term that results from the tensile centrifugal force, P_{M_1}, and the last term in Eq. (33). Intuitively, in order to increase the slope of $\omega_{n,c}$ with increasing n_s, one would attempt to increase the axial centrifugal forces through M_1 and L_1. Apart from the uniform reduction that higher inertia and length will cause to the modal frequency, the effect of the tensile load in the integral in Eq. (33) is counteracted by the last term in this equation that behaves as a negative virtual spring. This term corresponds to the transverse load acting on the tip mass due to the changing direction of the centrifugal force, as the cantilever tip mass vibrates. These opposing terms are both dependent on the centrifugal force (specifically on the product $M_1\Omega^2$), and as a result, an increasing rotational speed would affect them in the same way. Especially for larger rotational speeds where the magnitude of the integral is dominated by Ω^2, there is only a narrow potential for self-tuning. Note that this is valid both for "small" and "large" vibrations of the magnets. Therefore, the cantilever beam harvester is subject to a relatively low limit for the achievable slope, especially when high rotational speeds are considered.

In contrast, the concept proposed in Fig. 1 can overcome this limitation due to the presence of a non-vibrating tuning mass, without requiring increased inertia or space, and without needing structural elements to be replaced (e.g. beam thickness, width, material, etc.). By cross-examination of Eq. (33) with the proposed harvester's modal frequency in Eq. (27), one could notice that the terms responsible for tuning are augmented by the centrifugal force of the tuning mass, M_2, inherent to both P_1 and P_2. Since the tuning mass is not vibrating in the transverse direction, there is no tangential component of the centrifugal force, which disrupts the tuning in the cantilever example. Even though the last term in Eq.(33) is still present in Eq. (27), its negative action is overcome by the terms that depend only on M_2, entering the formula through both P_1 and P_2. Hence, the tuning mechanism attains a much higher potential for self-tuning.

To complete this analysis, time histories of the magnet's velocity and voltage are shown in Fig. 16 for the two juxtaposed concepts. For the cantilever beam counterpart, the case shown in Fig. 14 for $L_1 = 18$ mm is selected. The numerically computed time histories show that the cantilever beam concept exhibits a nearly regular resonance, whereas the proposed concept demonstrates an almost purely broadband output. Even though the resonant

response of the cantilever beam leads to higher peak voltage output due to the whole mass participating in electromagnetic interactions, this only occurs for a narrow frequency window, which in real-life applications with variable rotor speeds would be insufficient.

Figure 16

5 CONCLUSIONS

A novel concept for harvesting energy from torsional vibrations in rotor applications has been proposed. The dominant frequencies of typical torsional oscillations are proportional to the main rotor speed. The proposed concept utilizes centrifugal forces acting radially on a novel layout of thin beams to adjust the modal frequency of the harvester to the frequency of oscillations. The novelty lies in the distribution of harvester's inertia and in the introduction of a preload to overcome restrictions of existing harvester concepts. In particular, the presented concept uses a tuning mass at the outer support of the beams, which adjusts the self-tuning mechanism without affecting the vibrating inertia, and consequently avoiding adverse effects on the modal frequency. The preload has been shown to be useful for tuning the harvester to the lower speed range. The adopted self-tuning mechanism can offer high flexibility in adjusting a master design to a specific application (where torsional vibrations may follow different speed orders) without structural alterations (e.g. geometry and material of the beams). Numerical case studies for 1 x, 1.5 x and 2 x rotational speed orders were conducted. The studies showed the effectiveness of the self-tuned harvester to adjust its frequency to the expected order, whereas numerically computed time histories demonstrated its advantages in terms of the nearly purely broadband voltage and power output observed in a considerably wide frequency range. The proposed concept was also juxtaposed to a widely employed self-tuned harvester, based on a cantilever beam with a tip mass. The latter is limited mainly by the lateral components of the centrifugal forces, which effectively oppose the stiffening outcome of the tension imparted on the beams, leaving only the option of structural alterations to tune the cantilever harvester. However, the necessary corresponding downsizing of the beam thickness is incompatible with high rotor speeds from a material strength viewpoint. This limitation has been shown to be overcome by the proposed concept. Introduction of two independent parameters: the weight of the tuning mass and the magnitude of the preload allow greater flexibility in the design, leading to nearly constant voltage output within typical speeds of variable speed rotors.

ACKNOWLEDGEMENTS

The authors wish to express their gratitude to the Engineering and Physical Sciences Research Council (EPSRC) for the financial support extended to the "**Targeted energy transfer in powertrains to reduce vibration-induced energy losses**" [Grant number EP/L019426/1], under which this research was carried out.

REFERENCES

[1] N.G. Stephen, On energy harvesting from ambient vibration, *J. Sound Vib.* 293 (2006), 409–425.

[2] A. Marin, J. Turner, D.S. Ha, S. Priya, Broadband electromagnetic vibration energy harvesting system for powering wireless sensor nodes, *Smart Mater. Struct.* 22 (2013), 075008.

[3] G. Park, T. Rosing, M.D. Todd, C.R. Farrar, W. Hodgkiss, Energy harvesting for structural health monitoring sensor networks, *J. Infrastruct. Syst.* 14 (2008), 64–79.

[4] A.T. Eshghi, S. Lee, H. Lee, Y.-C. Kim, Parameter study and optimization for piezoelectric energy harvester for TPMS considering speed variation, *Proc. SPIE 9806*, *Smart Materials and Nondestructive Evaluation for Energy Systems 2016*, 98060Z (1 April 2016).

[5] G. Manla, N.M. White and M.J. Tudor, Numerical Model of a Non-Contact Piezoelectric Energy Harvester for Rotating Objects, *IEEE Sensors Journal*, 12 (2012), 1785-1793.

[6] A. Erturk and D.J. Inman, A Distributed Parameter Electromechanical Model for Cantilevered Piezoelectric Energy Harvesters, *J. Vibration Acoustics* 130 (2008), 041002 (15 pages).

[7] B.P. Mann and N.D. Sims, Energy harvesting from the nonlinear oscillations of magnetic levitation, *J. Sound and Vibration*, 319 (2009), 515-530.

[8] P. Alevras, S. Theodossiades and H. Rahnejat, Broadband energy harvesting from parametric vibrations of a class of nonlinear Mathieu systems, *Appl. Phys. Lett.* 110 (2017), 233901.

[9] P. Alevras, S. Theodossiades and H. Rahnejat, On the dynamics of a nonlinear energy harvester with multiple resonant zones, *Nonlinear Dyn* 92 (2018), 1271–1286.

[10] E.D. Niri and S Salamone, A passively tunable mechanism for a dual bimorph energy harvester with variable tip stiffness and axial load, *Smart Mater. Struct.* 21 (2012), 125025 (15pp).

[11] E.S. Leland and P.K. Wright, Resonance tuning of piezoelectric vibration energy scavenging generators using compressive axial preload, *Smart Mater. Struct.* 15 (2006), 1413–1420.

[12] Y. Cheng, N. Wu and Q. Wang, An efficient piezoelectric energy harvester with frequency self-tuning, *J. Sound and Vibration* 396 (2017), 69–82.

[13] A.H. Nayfeh and P.F. Pai, Linear and Nonlinear Structural Mechanics, Wiley, New York, 2004.

[14] L.N. Virgin, Vibration of Axially-Loaded Structures, Cambridge University Press, Cambridge, 2007.

[15] R.B. Bhat, Transverse vibrations of a rotating uniform cantilever beam with tip mass as predicted by using beam characteristic orthogonal polynomials in the Rayleigh-Ritz method, *J. of Sound and Vibration*, 105 (1986), 199-210.

[16] S. Naguleswaran, Lateral Vibration of a Centrifugally Tensioned Uniform Euler-Bernoulli Beam, *J. of Sound and Vibration* 176 (1994), 613-624.

[17] M. Li, Analytical study on the dynamic response of a beam with axial force subjected to generalized support excitations, *J. of Sound and Vibration* 338 (2015), 199–216.

[18] S. Lenci and G. Rega, Nonlinear Free Vibrations of Planar Elastic Beams: A Unified Treatment of Geometrical and Mechanical Effects, *Procedia IUTAM* 19 (2016), 35-42.

[19] S. Lenci, F. Clementi and G. Rega, A comprehensive analysis of hardening/softening behaviour of shearable planar beams with whatever axial boundary constraint, *Meccanica* (2016) 51, 2589–2606.

[20] L. Gu and C. Livermore, Passive self-tuning energy harvester for extracting energy from rotational motion, *Applied Physics Letters* 97 (2010), 081904.

[21] L. Gu and C. Livermore, Compact passively self-tuning energy harvesting for rotating applications, *Smart Mater. Struct.* 21 (2012), 015002 (9pp).

[22] M. Elhadidi, M. Helal, O. Nassar, M. Arafa and Y. Zeyada, Tunable bistable devices for harvesting energy from spinning wheels, *Proc. SPIE 9431, Active and Passive Smart Structures and Integrated Systems 2015*, 94310S (2 April 2015).

[23] Y.-J. Wang, T.Y. Chuang and J.-H.Yu, Design and kinetic analysis of piezoelectric energy harvesters with self-adjusting resonant frequency, *Smart Mater. Struct.* 26 (2017), 095037 (10pp).

[24] M. Li, Y. Wen, P. Li and J. Yang, A resonant frequency self-tunable rotation energy harvester based on magnetoelectric transducer, *Sensors and Actuators A* 194 (2013), 16– 24.

[25] J.-C. Hsu, C.-T. Tseng and Y.-S. Chen, Analysis and experiment of self-frequency tuning piezoelectric energy harvesters for rotational motion, *Smart Mater. Struct.* 23 (2014), 075013 (13pp).

[26] M. Guan and W.-H. Liao, Design and analysis of a piezoelectric energy harvester for rotational motion system, *Energy Conversion and Management* 111 (2016), 239–244.

[27] H.-X. Zou, W.M. Zhang, W.-B. Li, K.-X. Wei, Q.-H. Gao, Z.-K. Peng and G. Meng, Design and experimental investigation of a magnetically coupled vibration energy harvester using two inverted piezoelectric cantilever beams for rotational motion, *Energy Conversion and Management* 148 (2017), 1391–1398.

[28] Y. Zhang, R. Zheng, K. Shimono, T. Kaizuka and K. Nakano, Effectiveness Testing of a Piezoelectric Energy Harvester for an Automobile Wheel Using Stochastic Resonance, *Sensors* 16 (2016), 1727 (16 pages).

[29] H. Kim, W.C. Tai and L. Zuo, Self-tuning stochastic resonance energy harvester for smart tires, *Proc. SPIE 10595, Active and Passive Smart Structures and Integrated Systems XII*, 105950U (16 March 2018).

[30] Z. Chen, B. Guo, Y. Xiong, C. Cheng and Y. Yang, Melnikov-method-based broadband mechanism and necessary conditions of nonlinear rotating energy harvesting using piezoelectric beam, *J. of Intelligent Material Systems and Structures* 27 (2016), 2555–2567.

[31] S. Naguleswaran, Lateral Vibration of a Uniform Euler-Bernoulli Beam Carrying a Particle at an Intermediate Point, *J. of Sound and Vibration* 227 (1999), 205-214.

[32] B.A.M. Owens and B.P. Mann, Linear and nonlinear electromagnetic coupling models in vibration-based energy harvesting, *J. of Sound and Vibration*, 331 (2012), 922-937.

ACCEPTED MANUSCRIPT

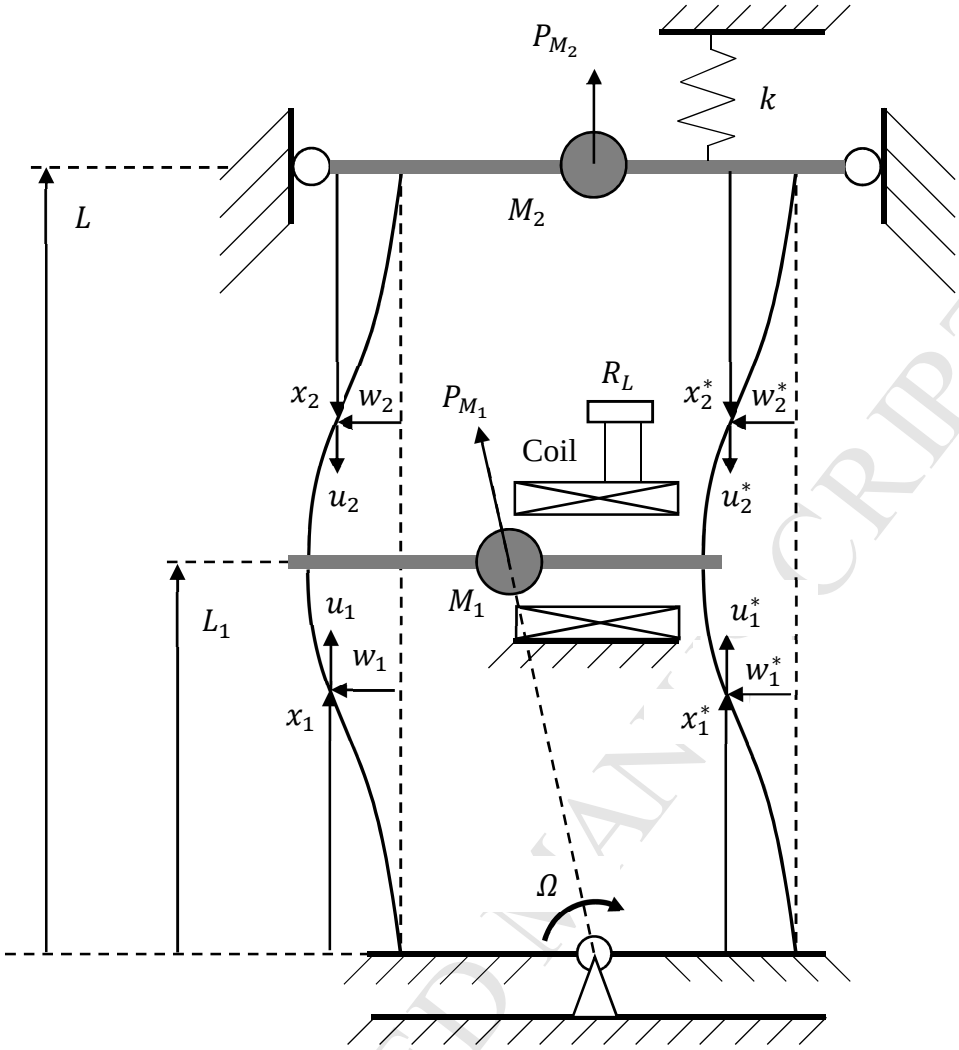

Fig. 1. Sketch of the proposed electromagnetic rotational energy harvester.

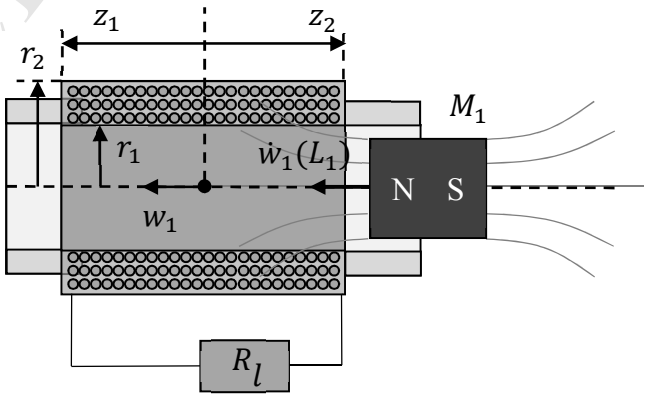

Fig. 2. Sketch of a magnet moving along the axis of a coil of wire.

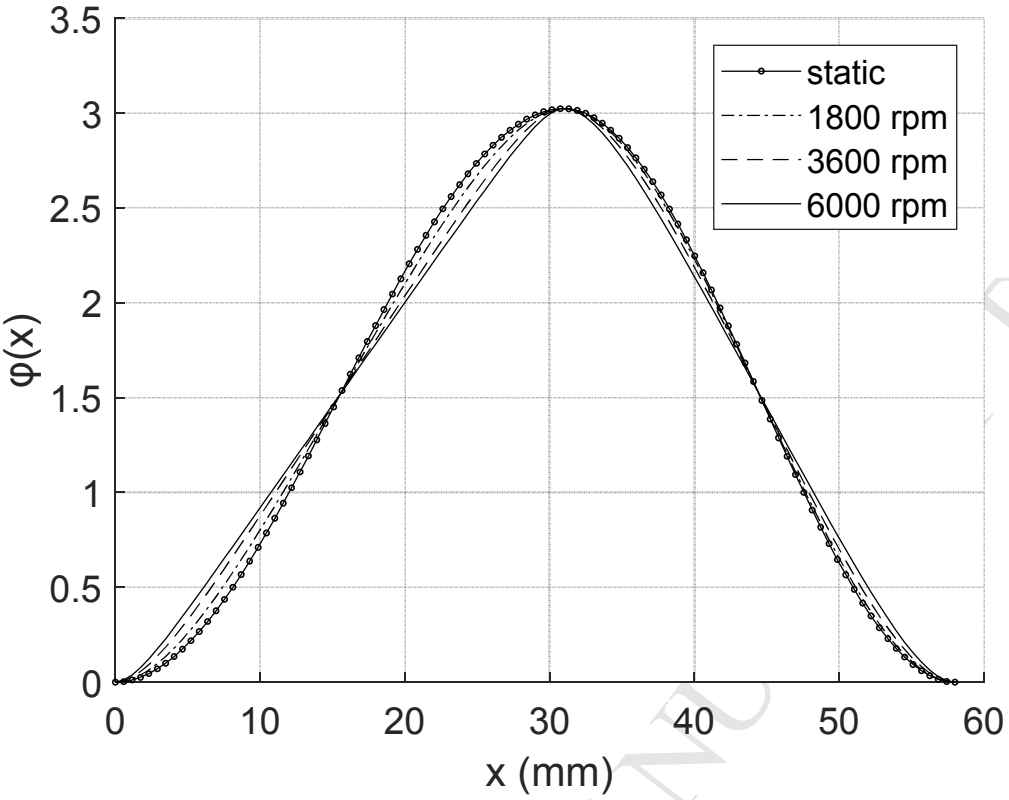

Fig. 3. Mode shapes of the beams for different rotational speeds. Case study computed for the parameter values listed in Table 1.

ACCEPTED MANUSCRIPT

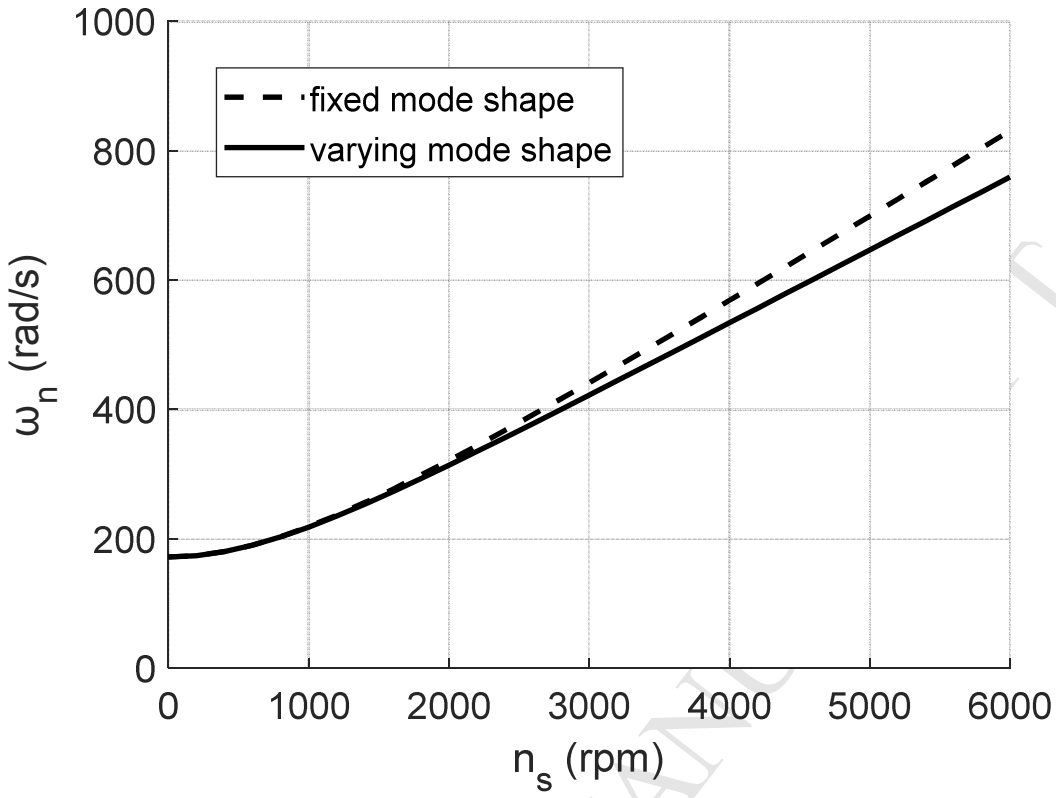

Fig. 4. Comparison of computing the harvester's first modal frequency using the herein described approach (————) and assuming a fixed mode shape (– – – –), for the parameters of Table 1.

ACCEPTED MANUSCRIPT

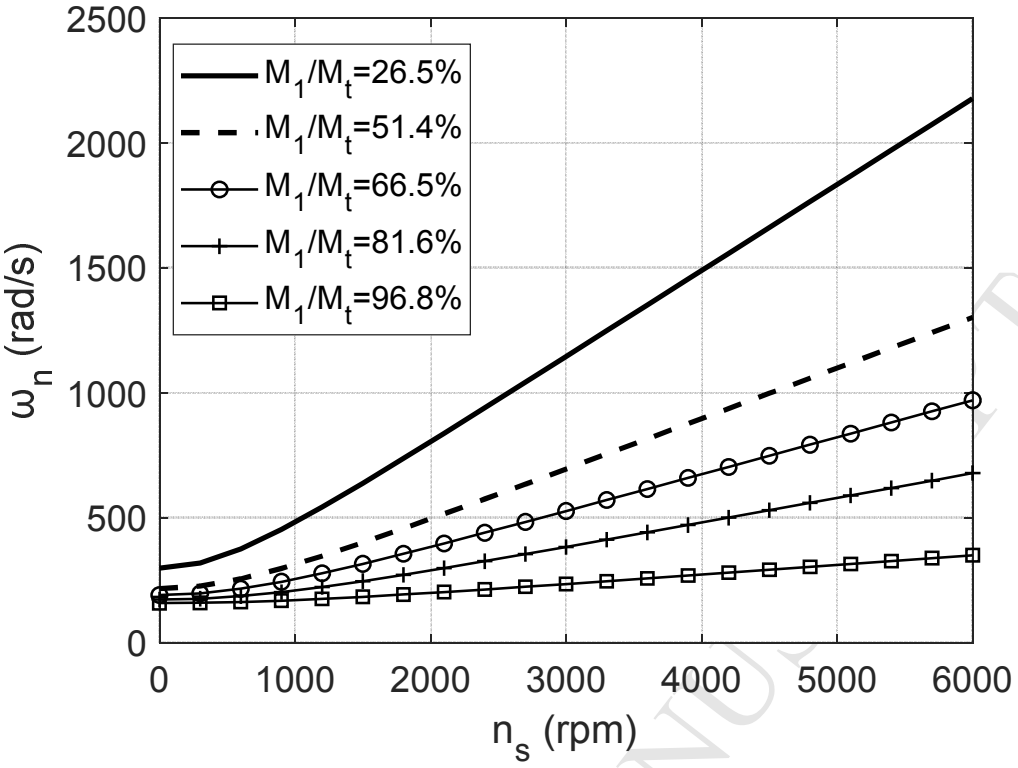

Fig. 5. Variation of the harvester's first modal frequency ω_n with increasing rotational speed n_s for a different distribution of mass M_1/M_t, and the parameters of Table 1.

ACCEPTED MANUSCRIPT

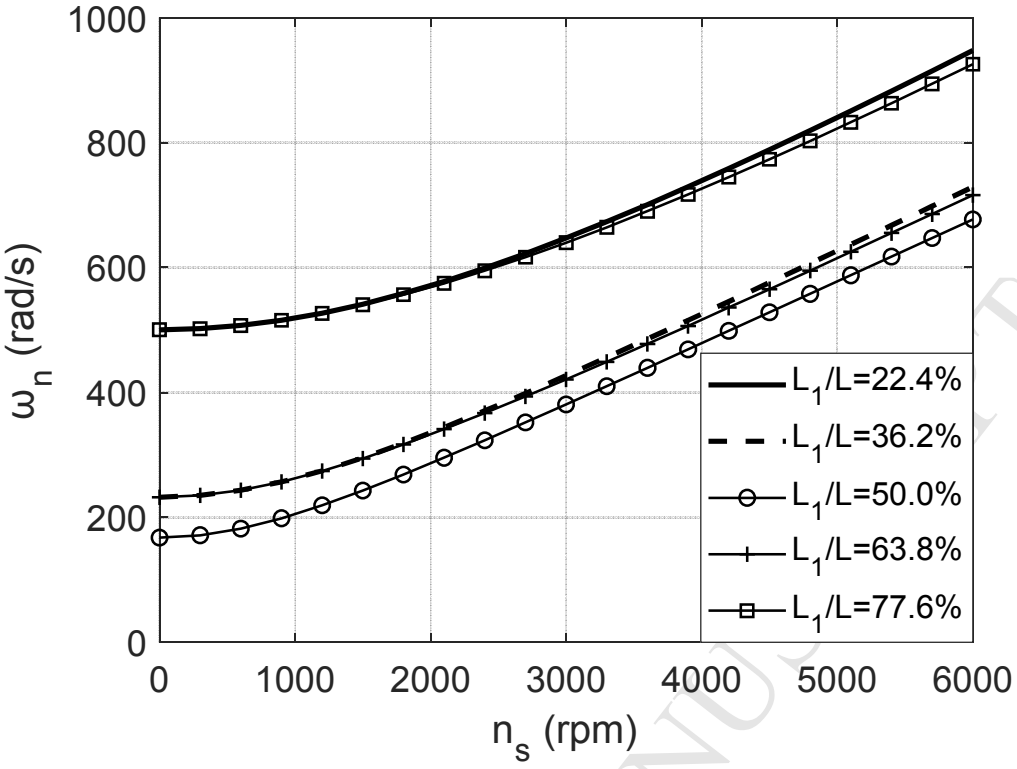

Fig. 6. Variation of the harvester's first modal frequency ω_n with increasing rotational speed n_s for a different positioning of the vibrating magnet L_1/L, and the parameters of Table 1.

ACCEPTED MANUSCRIPT

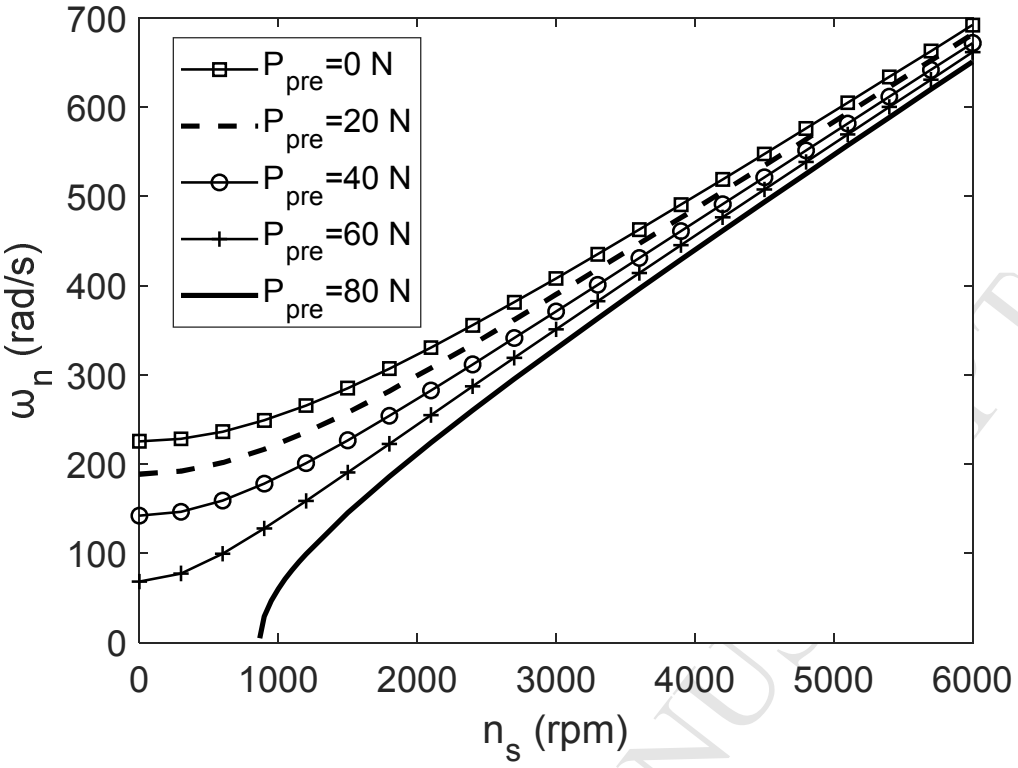

Fig. 7. Variation of the harvester's first modal frequency ω_n with increasing rotational speed n_s for different preloads P_{pre}, and the parameters of Table 1.

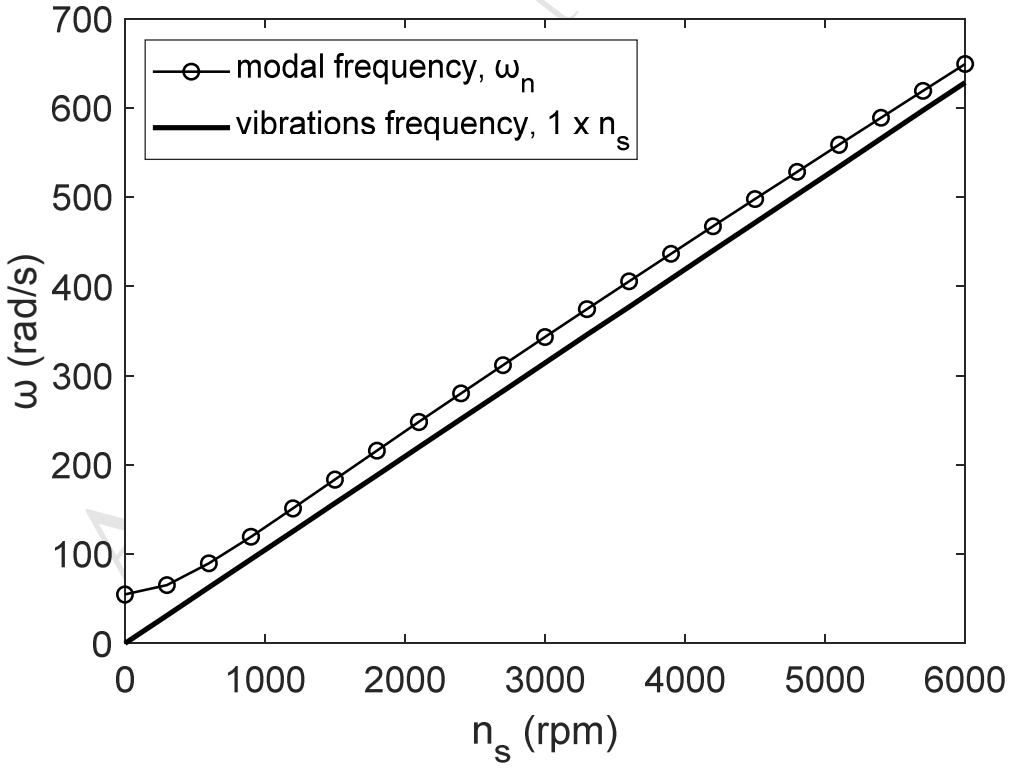

Fig. 8. Modal frequency of the self-tuned harvester for the first case study ($1 \times n_s$) using the parameters of Table 2 and: $M_1 = 0.149$ kg, $M_t = 0.182$ kg, $L_1 = 0.5L$, $P_{pre} = 60$ N.

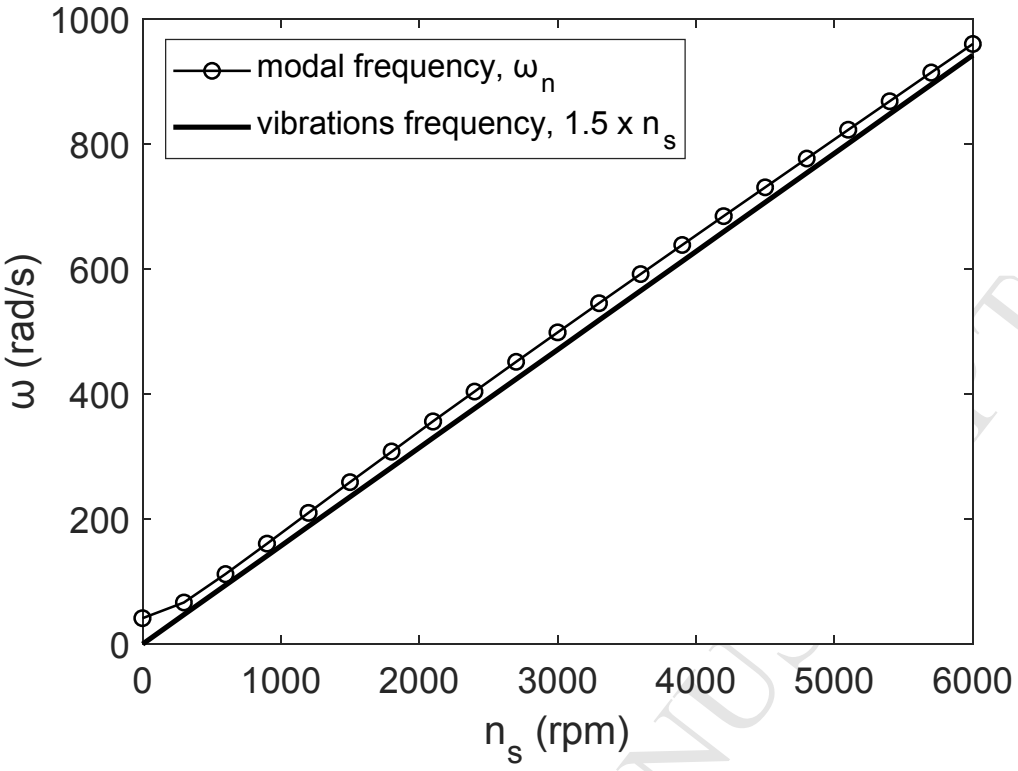

Fig. 9. Modal frequency of the self-tuned harvester for the second case study ($1.5 \times n_s$) using the parameters of Table 2 and: $M_1 = 0.12$ kg, $M_t = 0.182$ kg, $L_1 = 0.5L$, $P_{pre} = 62$ N.

ACCEPTED MANUSCRIPT

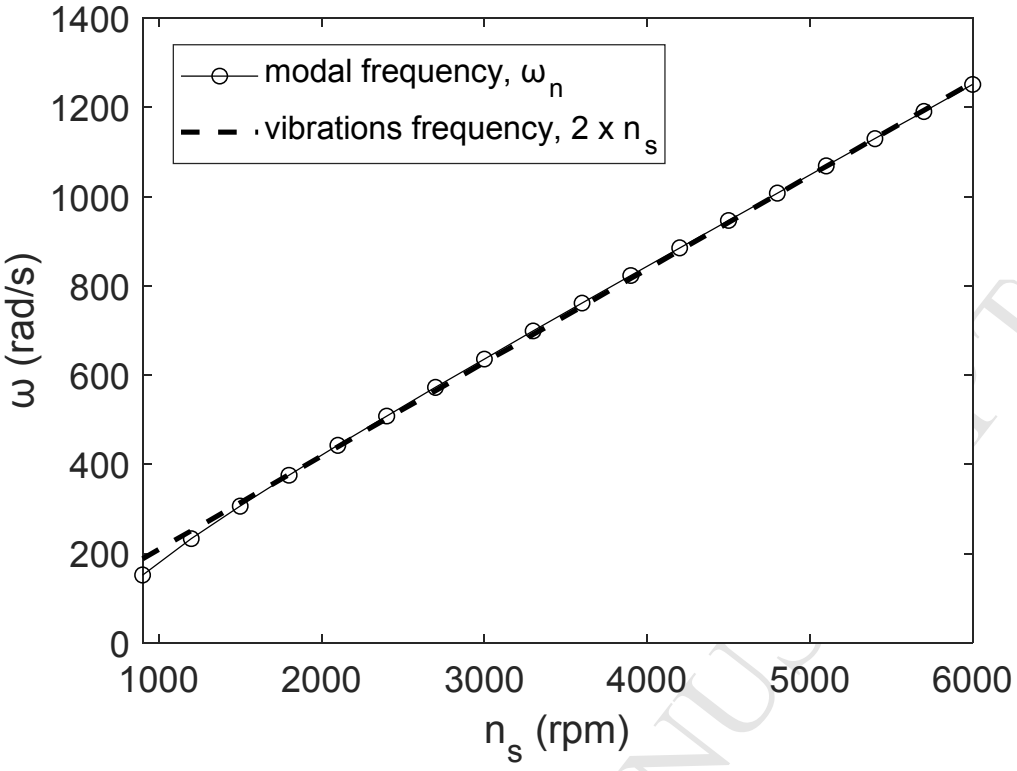

Fig. 10. Modal frequency of the self-tuned harvester for the third case study ($2 \times n_s$) using the parameters of Table 2 and: $M_1 = 0.095$ kg, $M_t = 0.182$ kg, $L_1 = 0.5L$, $P_{pre} = 85$ N.

ACCEPTED MANUSCRIPT

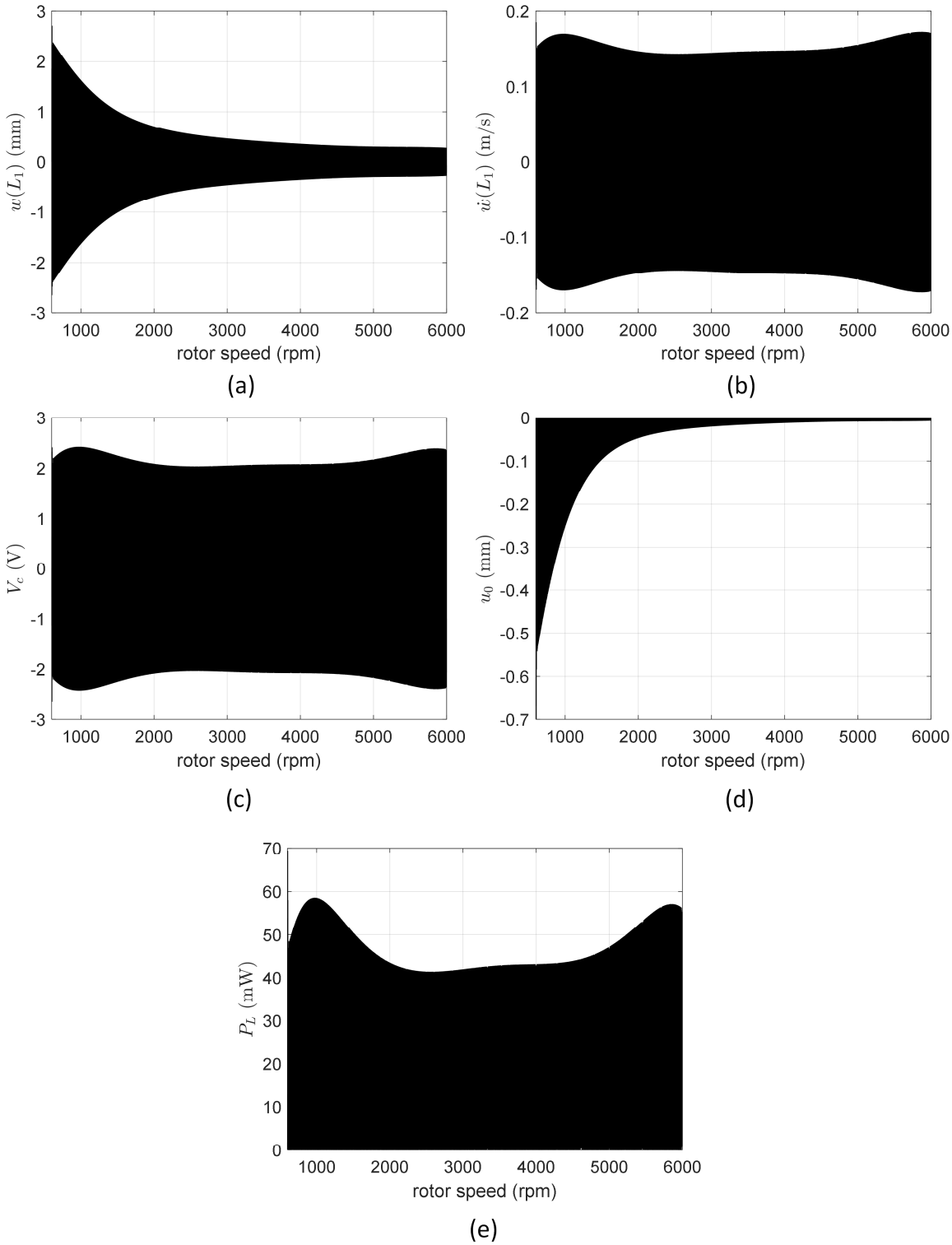

Fig. 11. Time history of the harvester response to $1 \times n_s$ vibrations by numerically integrating Eqs (30) – (32), using the parameters listed in Table 2 and $M_1 = 0.149$ kg, $M_t = 0.182$ kg, $L_1 = 0.5L$, $P_{pre} = 60$ N; (a) deflection of the vibrating magnet M_1; (b) velocity of the vibrating magnet M_1; (c) Voltage induced to the coil; (d) axial displacement of the beams' far-end support; (e) power delivered to the external electrical load R_L.

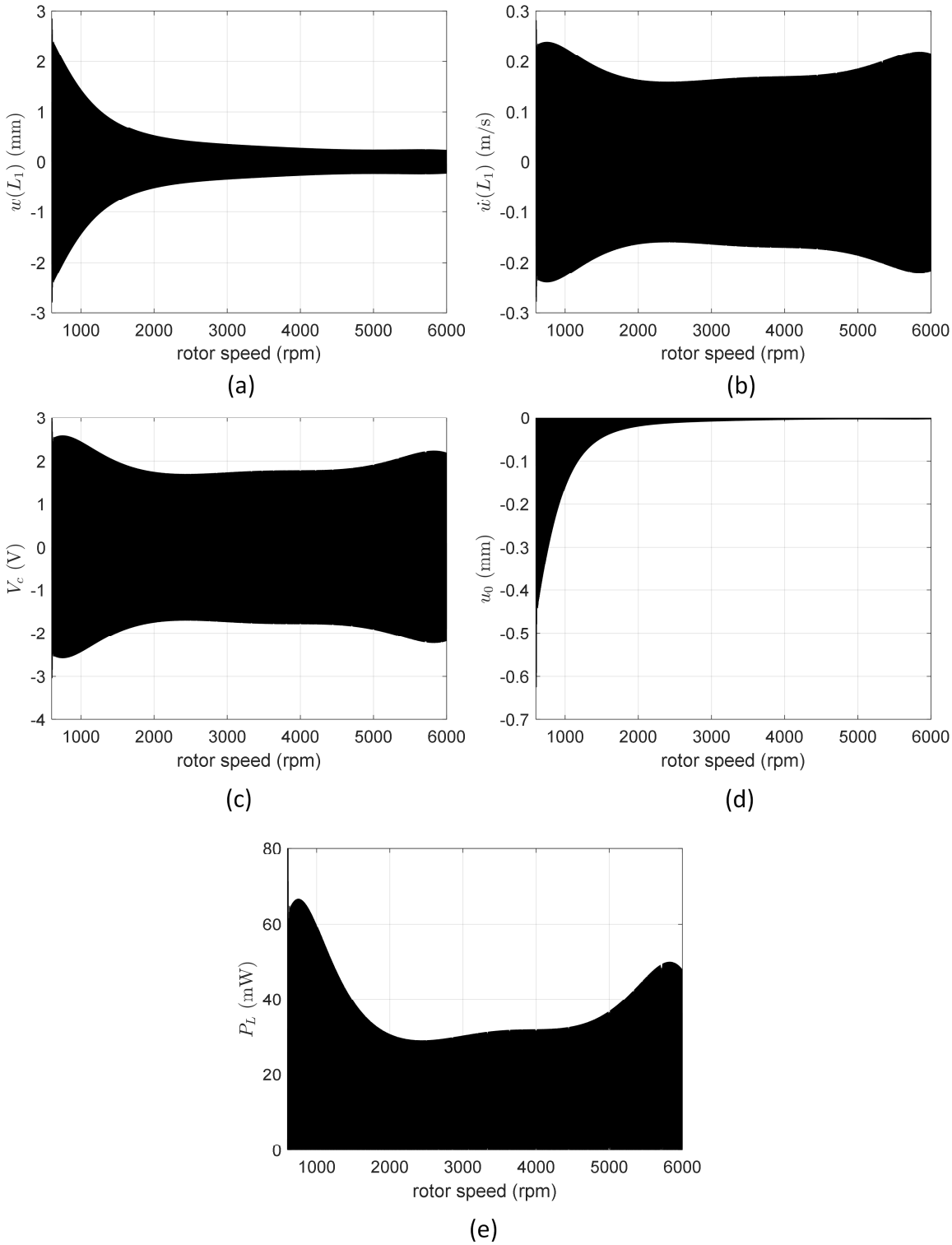

Fig. 12. Time history of the harvester response to $1.5 \times n_s$ vibrations by numerically integrating Eqs (30) – (32), using the parameters listed in Table 2 and $M_1 = 0.120$ kg, $M_t = 0.182$ kg, $L_1 = 0.5L$, $P_{pre} = 62$ N; (a) deflection of the vibrating magnet M_1; (b) velocity of the vibrating magnet M_1; (c) Voltage induced to the coil; (d) axial displacement of the beams' far-end support; (e) power delivered to the external electrical load R_L.

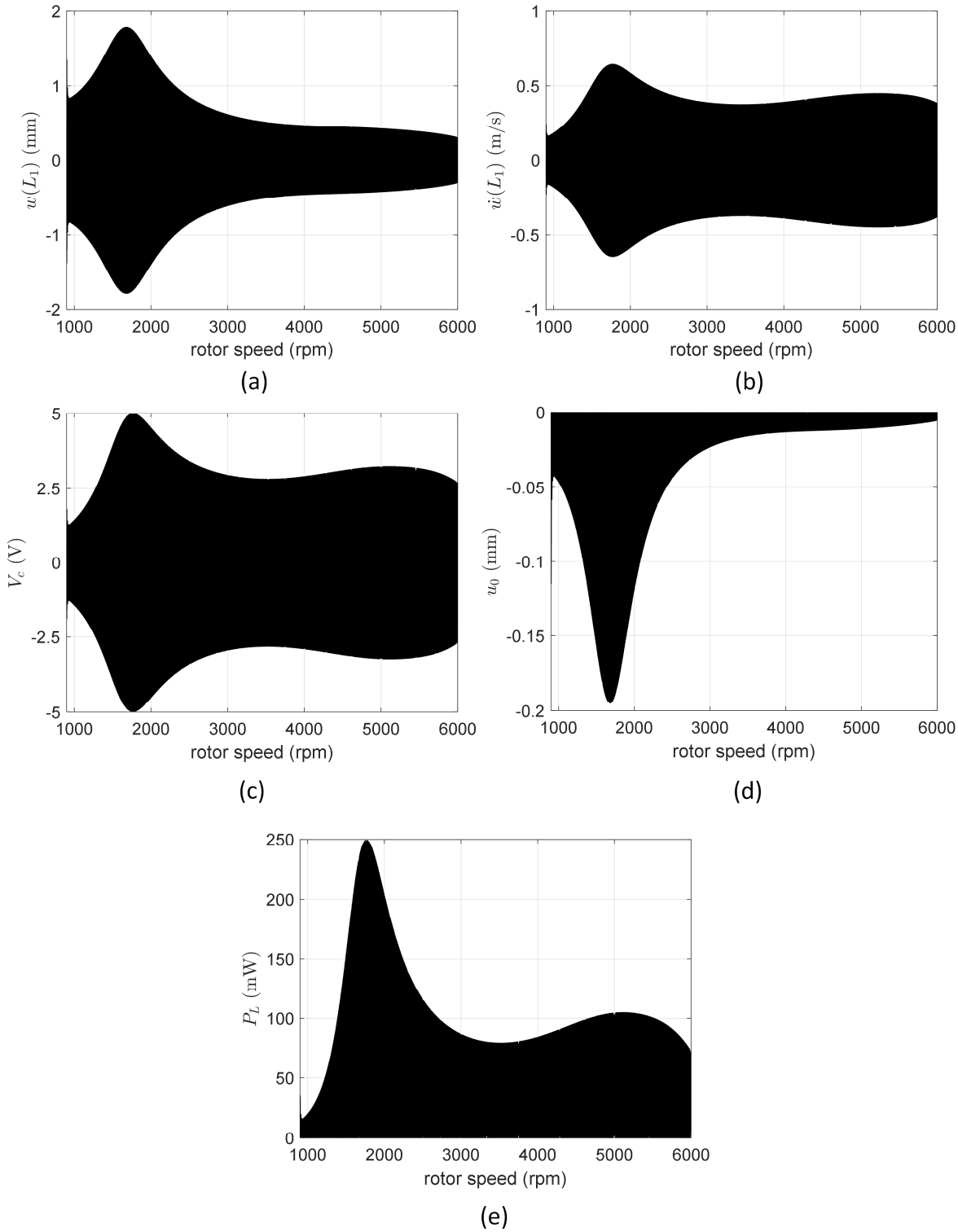

Fig. 13. Time history of the harvester response to $2 \times n_s$ vibrations by numerically integrating Eqs (30) – (32), using the parameters listed in Table 2 and $M_1 = 0.095$ kg, $M_t = 0.182$ kg, $L_1 = 0.5L$, $P_{pre} = 85$ N; (a) deflection of the vibrating magnet M_1; (b) velocity of the vibrating magnet M_1; (c) Voltage induced to the coil; (d) axial displacement of the beams' far-end support; (e) power delivered to the external electrical load R_L.

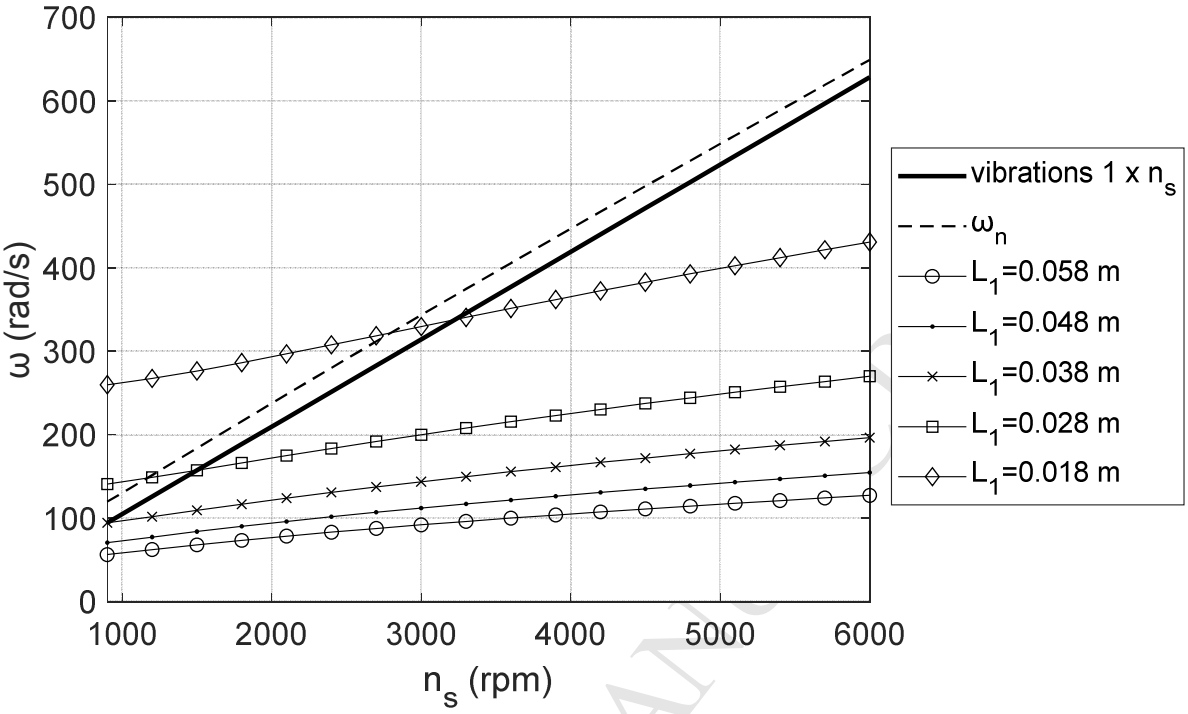

Fig. 14. Comparison of ω_n against $\omega_{n,c}$ for selected cantilever beam cases of $M_1 = 0.182$ kg and varying L_1, with the remaining parameters drawn from Table 2.

ACCEPTED MANUSCRIPT

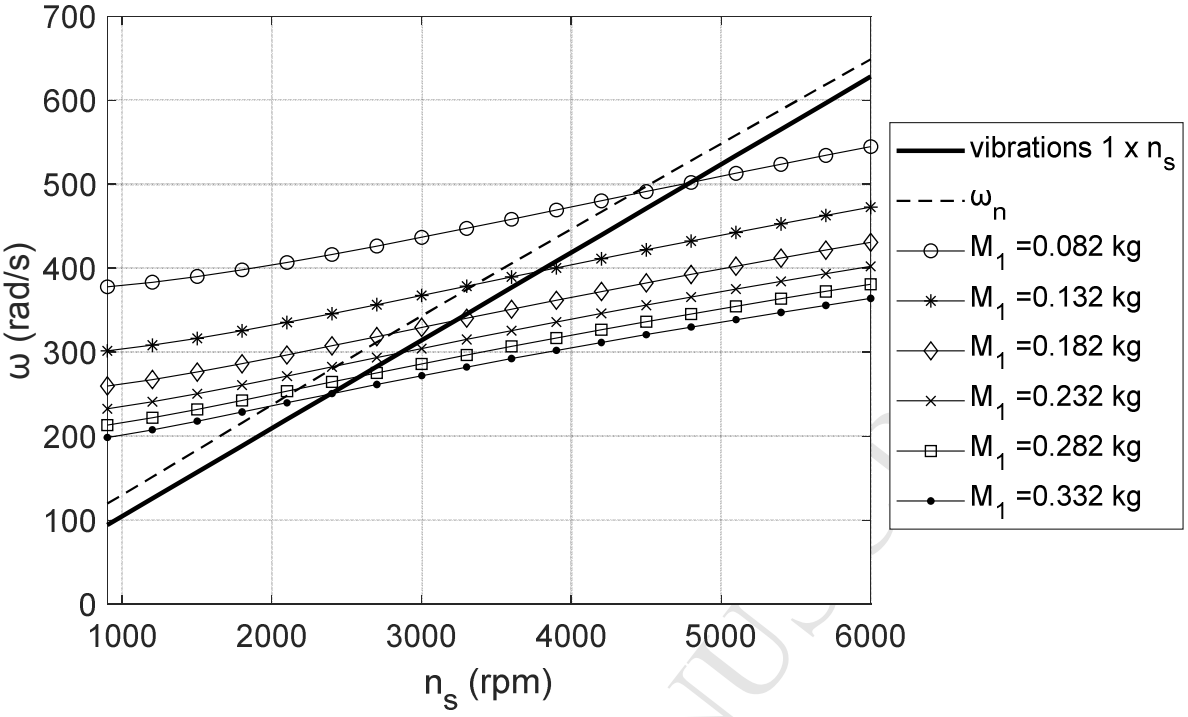

Fig. 15. Comparison of ω_n against $\omega_{n,c}$ for selected cantilever beam cases of $L_1 = 18$ mm and varying M_1, with the remaining parameters drawn from Table 2.

ACCEPTED MANUSCRIPT

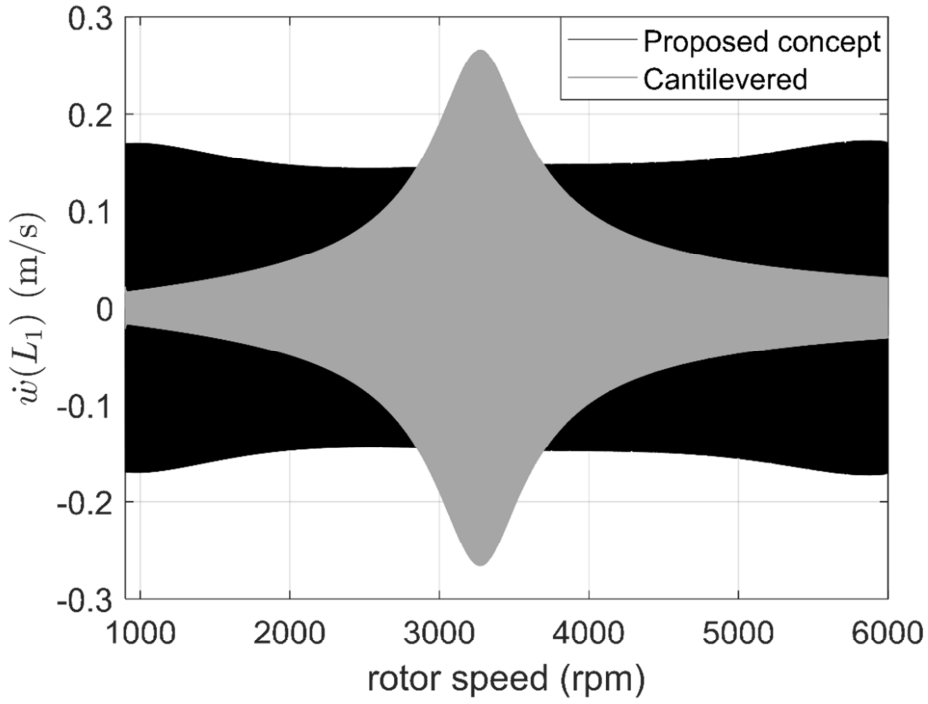

(a)

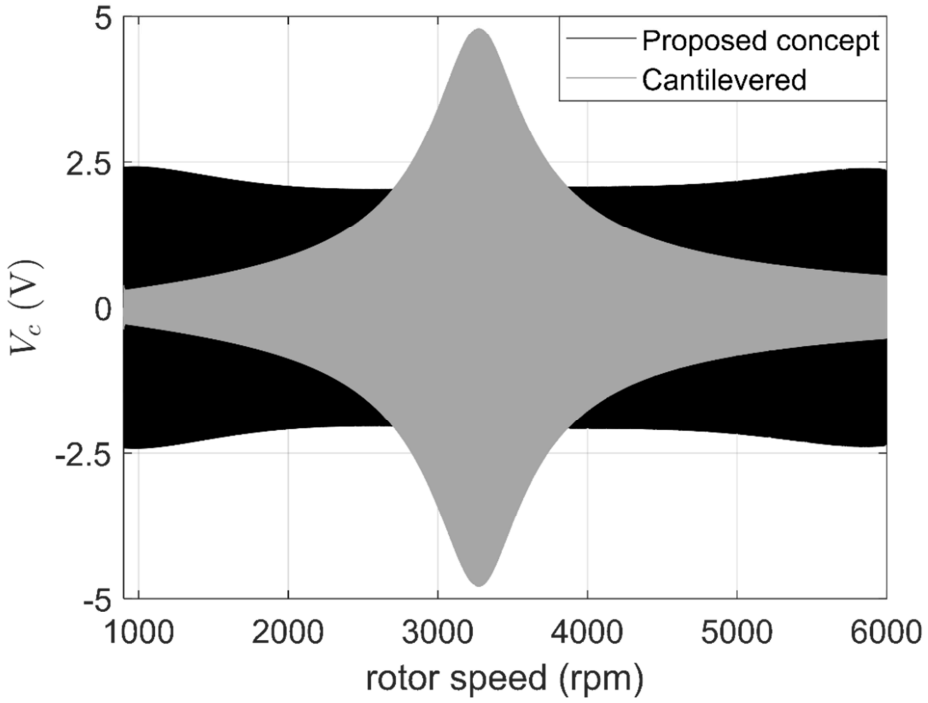

(b)

Fig. 16. Velocity and voltage time histories for the proposed concept and the cantilever beam counterpart for $1 \times n_s$. Results for the proposed concept are re-plotted from Fig. 11 for comparison purposes whereas the cantilever beam results correspond to $L_1 = 18$ mm in Fig. 14.